Univerzita Karlova v Praze
Matematicko-fyzikální fakulta

DIPLOMOVÁ PRÁCE

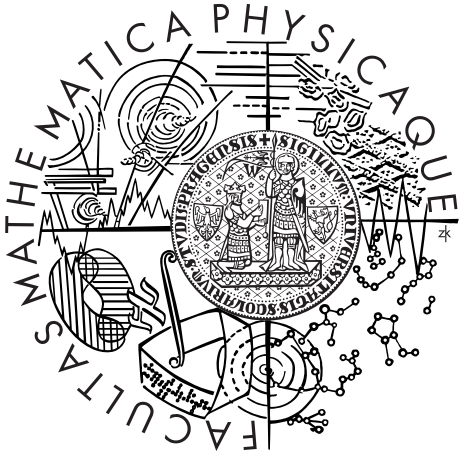

Denisa Kubániová

Studium vlivu příměsí na strukturní vlastnosti a stabilitu Langmuirových monovrstev mastných kyselin pomocí molekulových simulací

Katedra chemické fyziky a optiky

Vedoucí diplomové práce: RNDr. Martina Roeselová, Ph.D.

Studijní program: Fyzika

Studijní obor: Biofyzika a chemická fyzika

Praha 2014

Charles University in Prague
Faculty of Mathematics and Physics

MASTER THESIS

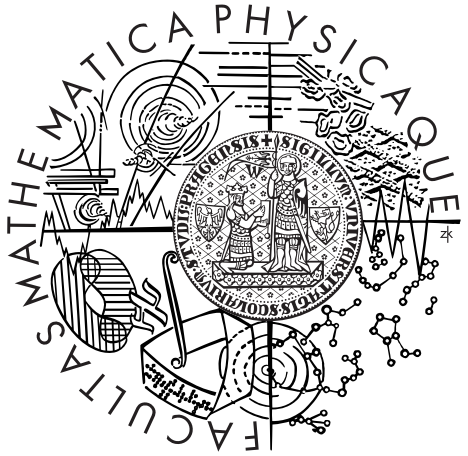

Denisa Kubániová

Molecular dynamics study of admixture influence on structural properties and stability of fatty acid Langmuir monolayers

Department of Chemical Physics and Optics

Supervisor of the master thesis: RNDr. Martina Roeselová, Ph.D.

Study programme: Physics

Specialization: Biophysics and Chemical Physics

Prague 2014

I would like to express my sincere gratitude to the supervisor of my master thesis, RNDr. Martina Roeselová, PhD., for guidance of my work, useful ideas when preparing the simulations and comments on the thesis. Furthermore, I acknowledge the helpful advice of Alena Habartová, PhD., concerning the preparation of the systems, simulation analysis and writing the thesis. Besides, I would like to thank the members of Computational Chemistry group of Prof. Pavel Jungwirth at Institute of Organic Chemistry and Biochemistry AS CR for a friendly environment in which the work was more like fun while investigating interesting problems.

Moreover I would like to thank my loved ones, mom Jarka and sister Dominika, who provided never ending support during the studies and throughout entire process of writing this thesis.

I declare that I carried out this master thesis independently, and only with the cited sources, literature and other professional sources.

I understand that my work relates to the rights and obligations under the Act No. 121/2000 Coll., the Copyright Act, as amended, in particular the fact that the Charles University in Prague has the right to conclude a license agreement on the use of this work as a school work pursuant to Section 60 paragraph 1 of the Copyright Act.

In Prague 31 July 2014 Denisa Kubániová

Názov práce: Studium vlivu příměsí na strukturní vlastnosti a stabilitu Langmuirových monovrstev mastných kyselin pomocí molekulových simulací

Autor: Denisa Kubániová

Katedra: Katedra chemické fyziky a optiky

Vedúci bakalárskej práce: RNDr. Martina Roeselová, Ph.D., ÚOCHB AV ČR

Abstrakt: Pomocí simulací molekulové dynamiky bylo studováno rozložení vybraných aromatických molekul, jmenovitě benzoové kyseliny a neutrální a zwitterionové formy L-fenylalaninu, ve třech systémech modelujících povrch kapaliny: a) vrstva vodného roztoku organických molekul, b) monovrstva palmitové kyseliny v kondenzovaném kapalném stavu na vodném roztoku organických molekul a c) monovrstva palmitové kyseliny ve stavu koexistence mezi kondenzovanou kapalnou fází a plynnou fází na vodném roztoku organických molekul. Pro všechny studované aromatické molekuly byla potvrzena povrchová aktivita a tendence k agregaci zejména na rozhraní voda-vzduch a voda-palmitová kyselina. Výsledky simulace provedené pro monovrstvu palmitové kyseliny na vodném roztoku benzoové kyseliny byly porovnány s publikovanými výsledky podobných simulací s jinou parametrizací. Srovnání ukázalo, že chování aromatických molekul na rozhraní voda-monovrstva mastné kyseliny silně závisí na použitém modelu. Strukturní vlastnosti Langmuirovy monovrstvy palmitové kyseliny byly vyhodnoceny na základě distibucí úhlu náklonu uhlovodíkových řetězců a analýzy dihedrálních uhlů v oblasti hlaviček palmitové kyseliny v závislosti na povrchové hustotě filmu a adsorbovaných aromatických molekulách. Simulace napodobující izotermální stlačování smíšené monovrstvy v Langmuirově cele měla za následek vytvoření vysoce uspořádaného klastru L-fenylalaninu v póru uvnitř monovrstvy. Provedené simulace poskytly informace na molekulární úrovni relevantní pro nedávno publikované experimentální studie smíšených aromatických-alifatických povrchových filmů.

Klíčová slova: fenylalanin, palmitová kyselina, hydrofobní kolaps, organický film, rozhraní voda-vzduch, surfaktant

Title: Molecular dynamics study of admixture influence on structural properties and stability of fatty acid Langmuir monolayers

Author: Denisa Kubániová

Department: Department of Chemical Physics and Optics

Supervisor: RNDr. Martina Roeselová, Ph.D., IOCB AS CR

Abstract: Using the classical molecular dynamics simulations, the interfacial partitioning of selected aromatic species, namely benzoic acid and neutral and zwitterionic form of L-phenylalanine, was studied in the three slab systems: a) aqueous organics solution, b) palmitic acid monolayer in tilted condensed phase at aqueous organics solution and c) palmitic acid monolayer in tilted condensed - 2D gas phase coexistence at aqueous organics solution. The surface activity and the tendency to aggregate in particular at the air-aqueous and palmitic acid-aqueous interface was confirmed for all of the investigated aromatic species. The results of the simulation performed for the system of palmitic acid monolayer at benzoic acid solution were compared with the literature results of a similar simulation that employed a different parametrization. The comparison showed that the behaviour of the aromatic species at the fatty acid monolayer-aqueous interface strongly depends on the force field. The structural properties of the palmitic acid Langmuir monolayers were evaluated by means of the chain tilt angle and the headgroup region dihedral angle distributions analysis depending on the surface film density and the adsorbed aromatic species. The simulations mimicking the isothermal compression of the mixed monolayer in the Langmuir trough resulted in the formation of a highly ordered L-phenylalanine cluster in a pore within the monolayer. The present simulations provided molecular level information relevant for the recently published experimental findings on mixed aromatic-aliphatic surfactant films.

Keywords: phenylalanine, palmitic acid, hydrophobic collapse, organic film, air-water interface, surfactant

Contents

Introduction

Water surfaces occurring on Earth are rich in various organic content originating from a variety of biogenic sources such as compounds resulting from the decomposition of dead aquatic animals and plants, and compounds produced by their biochemical reactions [1]. Some of the organic substances manifest an amphiphilic structure containing both a hydrophilic headgroup, strongly attracting the polar water molecules, and hydrophobic tailgroup, interacting with water only via significantly weaker dispersion interactions. This leads to the formation of various micellar structures in the aqueous environment as well as accumulation of the amphiphilic compounds at aqueous surfaces [2]. Palmitic and stearic acids are along with oleic acid the most common surface-active amphiphilic long-chain fatty acids found on ocean and fresh water surfaces and also on the surfaces of the aqueous aerosol droplets [3, 4]. These aliphatic molecules accumulate at the air-water interface and due to their amphiphilic behaviour tend to form insoluble monomolecular layers, called Langmuir monolayers after Irving Langmuir (1881–1957), whose pioneering work in chemistry of oil films on water [5] led to the formulation of a general theory of adsorbed films, awarded by the Nobel Prize in Chemistry in 1932.

Oxidized aromatic species released into the environment through anthropogenic emissions, including cases such as oil spills, are also an important component of marine aerosols [6]. The aromatics differ significantly in their hydrophobic structure (due to the presence of the aromatic ring) from the above mentioned biogenic surfactants, and due to adsorption at the interface, they modify the stability and morphology of the surface films [7]. The resulting diverse surface morphologies affect water uptake/evaporation, molecular transfer across the air-water interface, reactivity and optical properties of aerosol particles. Thus, this may lead to wide-ranging effects on the aerosol particles' impact on atmospheric chemistry and climate [8].

Simplified systems containing few compounds of those occurring at environmental interfaces are typically investigated in laboratory settings to get deeper understanding of surface layer characteristics in different states and conditions. In order to represent the complex composition of atmospheric aerosols, mixed films are more appropriate than homogenous monolayers. Mixed benzoic acid - stearic acid [9] and L-phenylalanine - stearic acid films at the air-aqueous interface [10] were recently studied by Langmuir through experiment combined with in-situ Brewster angle microscopy (BAM) and infrared reflection-absorption spectroscopy (IRRAS) by Griffith and coworkers in the laboratory of Professor Veronica Vaida at the University of Colorado at Boulder. By repeating compression-expansion cycles, structural properties and stability of the mixed films were examined, however, molecular-level information such as the exact distribution and protonation state of the compounds within the interfacial region could not be determined.

Compared to benzoic acid, L-phenylalanine has two hydrophilic groups (amine, -NH_2, and carboxyl, -COOH) instead of one. In the above experiments, modification of stearic acid monolayer deposited on an aqueous subphase containing either of the compounds was observed, but their effect is qualitatively

different. It was found that while both compounds adsorb to the aqueous - stearic acid interface, benzoic acid remains in the interfacial layer and modifies the stearic acid film within the compression-expansion cycles while adsorbed L-phenylalanine causes an early hydrophobic collapse of the stearic acid monolayer. It was suggested that this collapse is caused specifically by hydrophobic interactions between the aromatic ring of L-phenylalanine and the hydrocarbon tail of stearic acid, resulting in the splaying of the otherwise ordered tails of the stearic acid molecules and the formation of hydrophobic aggregates at the surface [10]. At this point, computer simulations of molecular dynamics can contribute to the knowledge about the processes taking place at the air-water interface in the presence of organics.

The objective of the present thesis is to perform molecular dynamics (MD) simulations of a model of a single-component monolayer composed of long-chain fatty acid deposited on aqueous solution of selected organic aromatic species, namely benzoic acid, neutral L-phenylalanine and zwitterionic L-phenylalanine. The selection of these particular organics was determined by several factors, the main of which was the availability of experimental data for these systems, which provided the motivation for the study, as well as the possibility for comparison of our molecular insight with experimental results.

This work addresses the following questions:

What is the partitioning of oxidized aromatics at the air-water interface coated with a fatty-acid film? How do oxidized aromatics distribute between the aqueous phase - polar headgroup region - hydrophobic tail region - outer interface?

How do the aromatics mix with aliphatic surfactants? In what way does the interaction of aromatics with, and possibly their intercalation into, the surfactant monolayer affect the monolayer structure and stability?

Is clustering of the aromatics important in these processes?

What is the morphology of the three-dimensional structures observed experimentally after collapse of the fatty acid monolayer?

How does the choice of the force field influence the behaviour of the aromatic species at the air-water or palmitic acid-water interface on L-phenylalanine solution subphase?

In the first chapter of the thesis theoretical background of the Langmuir trough experiment is given and the results of the measurements performed for the mixed benzoic acid - stearic acid and L-phenylalanine - stearic acid films at the air-aqueous interface are reviewed, followed by the chapter about the computational details of the simulated systems. Molecular dynamics simulations and subsequent analysis of their results allow us to provide answers to at least some of the above questions, discussed in detail in the Chapter 3 and briefly summarized in Chapter 4. All supporting information to the MD simulations are given in the Appendices.

1. Langmuir trough experiment

A Langmuir trough [11] is an experimental apparatus allowing to prepare and investigate properties of the insoluble monolayers of amphiphilic surfactants spread onto an aqueous subphase (Langmuir monolayers). The surface covered by the surface active molecules can be continuously compressed and expanded by the moving barriers, and thus the molecular density or equivalently, the mean area per molecule is modified. This is performed repeatedly at the constant temperature, giving rise to the isotherm compression-expansion cycles.

The effect of the monolayer on the surface pressure of the interface in different stages of the cycle is measured by a Wilhelmy plate partially immersed in the liquid. The surface pressure is defined as the difference of the surface tension of the pure subphase γ_0 and the surface tension γ of the subphase with surfactant which lowers the surface tension,

$$\pi = \gamma_0 - \gamma. \tag{1.1}$$

The variation of the surface pressure π with the molecular area A is graphically represented by the surface pressure – area (π-A) isotherm as depicted in Figure 1.1.

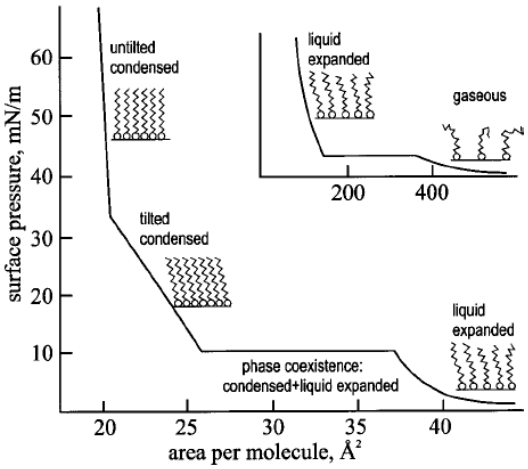

Figure 1.1: Typical π-A isotherm and molecular configurations in different regions separated by the phase transitions, adapted from [11]

As the monolayer is compressed (or expanded), the various two-dimensional phases predominantly occur in the system depending on the mean area per molecule. The 2D phases are separated by phase transitions, when both phases coexist in equilibrium and the surface pressure remains constant while the molecular area changes. For the very small concentrations of the surfactant at the air-aqueous interface the molecules execute a random motion similar to the motion of ideal-gas molecules enclosed in a container. Decrease in the surface area brings the surfactant molecules close together, leading to the formation of monolayer in the liquid expanded phase. The tendency of the amphiphilic molecules to create the monolayer on the aqueous solution is led by the reduction in the surface energy, or equivalently, surface tension of the solution. The continuing

compression increases the density of the film and the surfactant molecules arrange themselves to a close-packed array, the liquid condensed phase. Once the tilted and, subsequently, the untilted condensed phase has been reached, if the area is further reduced, the collapse of the monolayer occurs. It leads to the formation of hydrophobic aggregates of complex morphologies, accompanied by the sharp drop of the surface pressure in the π-A isotherm.

In addition to the π-A isotherm measurements providing thermodynamic information, structural analysis and surface-sensitive experimental techniques like x-ray diffraction (XRD), infrared reflection-absorption spectroscopy (IRRAS) and Brewster angle microscopy (BAM) gave the experimentalists powerful tools to directly probe the air-aqueous interface and enabled a deeper understanding of the structures and the two-dimension phase transitions occurring in these systems.

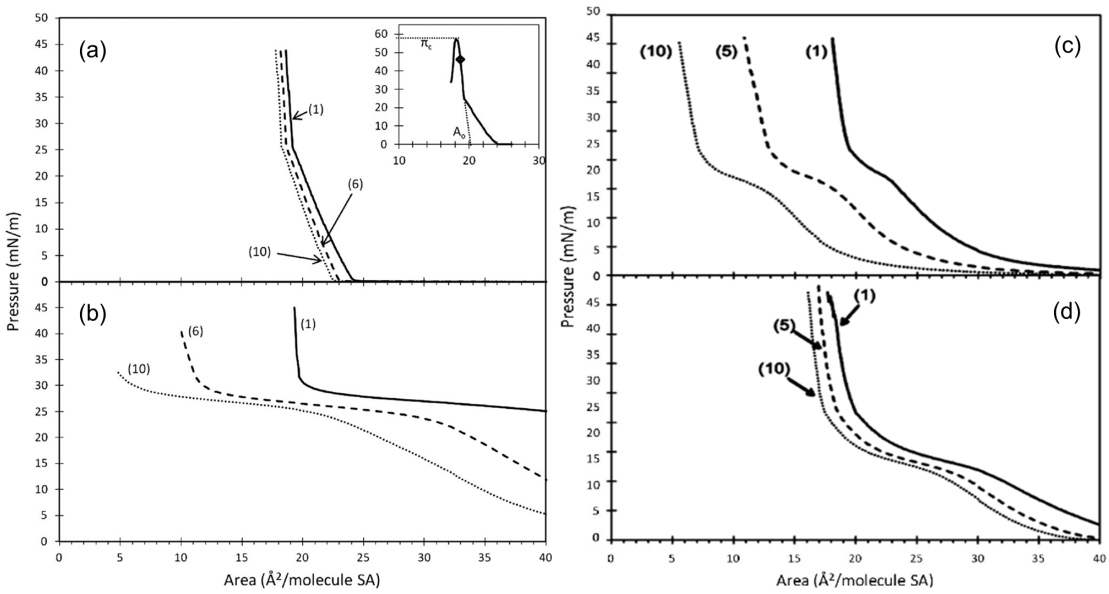

Figure 1.2: Selected compression π-A isotherms cycles (as indicated by numbers) from 10 compression-expansion cycles, (a) stearic acid at water subphase, (b) stearic acid at L-phenylalanine aqueous solution subphase [10], (c) stearic acid at benzoic acid aqueous solution subphase and (d) stearic acid at benzaldehyde aqueous solution subphase [9]. Inset in (a) shows a typical stearic acid isotherm at water subphase past the point of collapse, with the molecular footprint A_0, collapse pressure π_c and maximum pressure for the isotherm cycles ◆. Courtesy of Elizabeth Griffith.

In the Langmuir trough experiments performed by Griffith et al. [9, 10], the amphiphilic molecules (stearic acid) dissolved in organic solvent were deposited dropwise on the surface of aqueous organics solution in the Langmuir trough with the barriers in the fully open position and equilibrated for 20 minutes to allow the solvent to evaporate and the surfactant molecules spread uniformly over the interface leading to the formation of the monolayer. When the surface pressure had stabilised, ten isotherm compression-expansion cycles were performed with constant barrier speed of $100\,\mathrm{cm}^2/\mathrm{min}$. A limit was set for the maximum surface pressure so as the film does not reach the collapse during the measurement. The evolution of the compression π-A isotherms with progressing compression-expansion cycles is shown in Figure 1.2.

A particular isotherm curve depends on the temperature and the composition of the system. For stearic and palmitic acid monolayers on water at the room temperature the 2D disordered gaseous phase passes directly into the tilted condensed phase with decreasing area per molecule, i.e. the liquid expanded phase is not present. The characteristic molecular area (or footprint A_0), defined as the extrapolation of the untilted condensed phase part of the isotherm to the zero surface pressure, is used here to compare the behaviour of various systems in the course of the isotherm cycles. The small decrease in the footprint value for the stearic acid monolayer deposited on pure water (Figure 1.2a) is caused by minor loss of stearic acid molecules from the interface during the cycles without the monolayer disruption, as seen from the small shift of the isotherms to lower π while their slopes remain unchanged.

Griffith et al. observed modification of the stearic acid monolayer by adsorption of three different oxidized aromatic species - benzaldehyde (Figure 1.2c), benzoic acid (Figure 1.2c) and L-phenylalanine (Figure 1.2b). All the above mentioned aromatics adsorb to the aqueous - stearic acid interface, but the effect on the monolayer is qualitatively different. The adsorbed L-phenylalanine significantly disrupts the film, evidenced by the loss of the stearic acid monolayer character of the isotherms (decrease of A_0) and a decrease in slope of the untilted condensed phase signifying a decline in phase stability. The stearic acid monolayer undergoes irreversible change through induced surface pressure causing an early hydrophobic collapse of the monolayer [10]. The benzaldehyde, the hydrophilic group of which is less oxidized than the carboxylic group of the benzoic acid, has lower propensity to hydrogen bonding with water and/or the fatty acids headgroups. Thus it is rather more likely to be squeezed out from the monolayer to the gas phase than to be retained in the stearic acid film, resulting in only small disruption of the monolayer. On the other hand, the benzoic acid is much less volatile and remains in the interfacial region, forcing more permanent modifications of the stearic acid film, evidenced by the significant decrease in A_0 with repeating isotherm cycles, even though the slopes remain consistent [9]. In contrast with the complete loss of stability of the stearic acid film seen with the L-phenylalanine, no such phenomenon was observed with the benzoic acid present in the system.

According to these studies, the large hydrophobic group of the aromatic species so different from the aliphatic structure of the fatty acid molecules deposited on the air-aqueous interface should facilitate the adsorption and the initial phase of the film disruption, while the modification during the isotherm cycles is likely to be affected by the hydrophilic headgroups changing the surface pressure. However, the detailed mechanism has not yet been introduced for the interplay between these groups. By employing the simulations of molecular dynamics we attempt to clarify processes taking place at the air-aqueous interface in these system both in the "open barrier position" of the Langmuir through as well as during the isotherm compression cycle.

2. Molecular simulations

Simulations of molecular dynamics (MD) stand somewhere between experimental investigation and theoretical predictions, being neither the former nor the latter. We can refer to them as computational experiments, performed on a model which captures main features of the investigated problem, sufficiently describing a real chemical system at the chosen level of approximation. MD simulations reach the spacial and time scales not easily achievable by experiment and thus may provide molecular insight complementary to the macroscopic experimental results and in some cases even predict the behaviour of systems in unfeasible experiments (extreme temperatures, pressures, unstable and artificial structures, etc.).

In MD simulations, one assumes validity of the Born-Oppenheimer approximation - atomic nuclei are moving at the potential energy surface (determined by other nuclei with their electron clouds) and the electrons instantaneously follow their movement. The atoms are represented by "soft" spheres with point charges in their centres moving according to the Newton laws and the interaction potential. As it is almost impossible to obtain the full multidimensional interaction potential even for a very simple system, it is usually approximated by a functional form with a set of parameters (force field) fitted to the ab-initio or experimental data. More details on the interaction potentials used in this work are given in Appendix A.

In addition to the Born-Oppenheimer approximation, we assume that the investigated systems obey the ergodic theorem - i.e. the averaging over the statistical ensembles equals to the time averaging over the trajectory, which should sufficiently sample the phase space. Single MD trajectory is then used to determine macroscopic thermodynamic properties of the simulated system.

2.1 Simulated systems

To model long-chain fatty acid monolayer deposited on aqueous solution of selected organic aromatic species we chose palmitic acid ($CH_3(CH_2)_{14}COOH$, Figure 2.1) instead of experimentally investigated stearic acid ($CH_3(CH_2)_{16}COOH$) since we had a pre-equilibrated model of the palmitic acid monolayer on aqueous subphase available and the performance of this model was well characterised in previous molecular dynamics simulations with various force fields [12]. Choice of

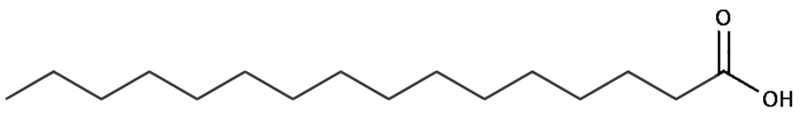

Figure 2.1: Schematic depiction of the palmitic acid molecule

the fatty acid with a somewhat shorter carbon chain is not expected to influence significantly the interactions with the aromatic species as it is known that fatty acids with chains from 13-14 up to 32 carbon atoms long form stable monolayer

at the aqueous surface [13]. In addition, palmitic and stearic acid exhibit similar characteristics, e.g. the π-A isotherms, chain tilt angle etc., and thus the overall behaviour of the system is preserved. In particular, palmitic acid monolayer on aqueous subphase exhibits the same hydrophobic collapse driven by external pressure typical for stearic acid.

The set of the palmitic acid monolayer systems with various values of mean area per palmitic acid molecule available from previous work [12, 14] was obtained by gradual compressing the lateral dimensions (x and y) of the simulation box while preserving the x:y ratio of 1 (see Figure 2.2).

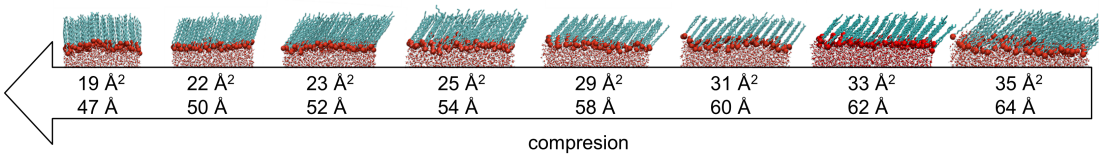

Figure 2.2: Snapshots of palmitic acid monolayer at the air-water interface in different compression stages, mean areas per palmitic acid molecule in Å^2 (top line) with the corresponding lateral box dimension in Å (bottom line). Aliphatic chains are rendered in cyan while carboxylic headgroups are shown as red beads. Courtesy of Alena Habartová [14].

Benzoic acid and L-phenylalanine (Figure 2.3) were chosen as the representative aromatic species in aqueous solution because of their atmospheric and environmental relevance, previously observed surface activity and water solubility even while exhibiting hydrophobic behaviour at the same time.

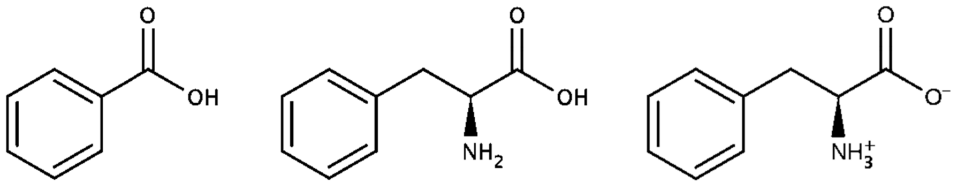

Figure 2.3: Schematic depiction of the aromatic molecules - benzoic acid (left), neutral L-phenylalanine (middle) and zwitterionic L-phenylalanine (right)

System with benzoic acid aqueous solution was simulated to test the MD simulation results of reference [9]. The L-phenylalanine molecule shares the same aromatic structure as well as the carboxylic functional group with benzoic acid, but in addition has an amino group that makes the solute - solute, solute - fatty acid monolayer, and solute - water interactions present in the system more complex. For this reason, L-phenylalanine represents a natural step in the series of increasing system complexity. Moreover, experimental results for L-phenylalanine are provided by the work of Griffith et al. [10], whereas MD investigation has not been performed yet.

Ionization state of the organic compounds with titratable groups can, in general, differ in the interfacial region from that in bulk aqueous solution, depending on the local environment the molecules experience [15]. L-phenylalanine, having

two such groups - acid (carboxyl group) and base (amino group) - can deprotonate and protonate, respectively, depending on the pH of the environment, which in turn will influence the interactions between L-phenylalanine and various compounds of the system. Using the classical MD simulations we cannot directly observe these transformations of the molecular character, which are related to the change in electronic structure and are the domain of ab initio and density functional theory approaches. However, we can observe the preference of different protonation states of L-phenylalanine to intercalate and mix with the surfactant monolayer resulting in changes in the distribution of oxidized aromatics between the aqueous phase, polar headgroup region, hydrophobic tail region and outer interface. Taking this into account, we decided to include two forms of L-phenylalanine in our study - the neutral one (Figure 2.3, middle) and the zwitterionic one (Figure 2.3, right). While the zwitterion is the prevalent form in the aqueous environment within a broad range of pH, the neutral form was included as an extreme to investigate the possible effect of the change in the protonation state on L-phenylalanine intercalation into the monolayer.

2.2 Interaction potentials

Benzoic acid topology was taken from ATB repository [16]. Gas phase geometry optimization was performed at the B3LYP/6-31G*. Bonding and non-bonding parameters were taken from GROMOS 53A7 parameter set [17]. Initial charges were estimated using the electrostatic potential (ESP) method of Merz-Kollman [18, 19] and final charges and charge groups generated by RESP fitting [20].

The geometries of the palmitic acid and the neutral L-phenylalanine molecules were optimized employing the Møller-Plesset second-order perturbation theory (MP2) in conjunction with the 6-31G* basis set by Gaussian 09 software suite [21, 22]. The zwitterionic L-phenylalanine was optimized by the Hartree-Fock method (HF) with the same basis set. The HF ESP calculation with 6-31G* basis set at the optimal geometries, followed by the RESP fitting [20], was used to obtain the partial charges at the atomic sites. For neutral L-phenylalanine the standard charges assigned by the OPLS force field were used in the end, as these charges differ only at the third decimal digit from the RESP-calculated ones while for the palmitic acid and zwitterionic L-phenylalanine the RESP refined charges were adopted. Bonding and non-bonding (Lennard-Jones) force field parameters were taken from all-atom OPLS parameter set [23]. SPC/E model [24], which incorporates three charges positioned at atomic sites, was used for water molecules. The force field parameters for all molecules are given in Appendix B.

Simulated systems were prepared using GROMACS tools [25, 26] and VMD graphical and scripting environment [27, 28]. All simulations presented here were performed in slab configuration with 3D periodic boundary conditions (PBC) as depicted in Figure 2.4. Periodic images of the slab configuration were placed so as to create infinite system surrounding the central simulation cell, with the slab extended in x and y dimensions and large enough distance between the surfaces of the slab's periodic images in the z direction to ensure their interaction via

long-range electrostatic forces to be negligible. This configuration of the model system is to mimic the surfactant monolayer at the aqueous organics solution in the Langmuir trough experiment.

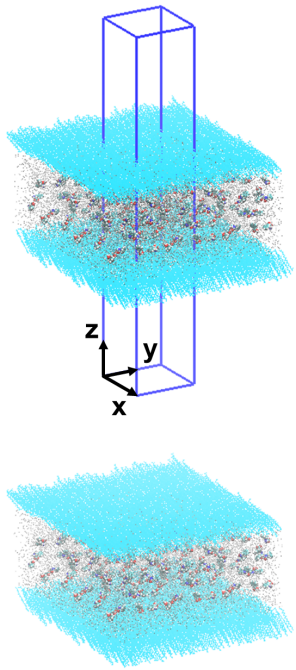

Figure 2.4: Periodic boundary conditions applied to the unit cell showing one periodic image of the simulated slab system in the z direction

2.3 System preparation

2.3.1 Surface of aqueous organics solution

20 molecules of one of the aromatic species (benzoic acid, neutral L-phenylalanine or zwitterionic L-phenylalanine) were placed on a regular grid and solvated using a pre-equilibrated box of SPC/E water molecules available in Gromacs to obtain the system of dimensions $52 \times 52 \times 68\,\text{Å}^3$. This system was subsequently centered within a box of the height of 300 Å, to prepare a slab with a vacuum layer above and below. Various slab thicknesses in the z direction were tested to prevent occurrence of unphysical solute "chains" throughout the solution slab, connecting its two interfaces together. Slab thickness of 68 Å was determined to be suitable for all further simulations. This choice led to a total of 5977 water molecules for benzoic acid aqueous solution, 5917 for neutral L-phenylalanine and 6381 for zwitterionic L-phenylalanine solution.

Benzoic acid solubility in water at 25 °C is $2.9\,\text{g/l} = 0.025\,\text{mol/l}$. Concentration of benzoic acid in our system is $0.20\,\text{mol/l}$. Similar enhanced concentration of benzoic acid was used in reference [9] to increase dynamics of the simulation as with smaller concentration the events of interest would be very rare. L-phenylalanine solubility in water at 25 °C is $29.6\,\text{g/l} = 0.18\,\text{mol/l}$. The same concentration was used in our simulations.

2.3.2 Tilted condensed phase of palmitic acid monolayer at aqueous organics solution subphase

Two monolayers of 116 palmitic acid molecules aligned in a hexagonal lattice with a mean area of 23 Å^2/molecule (Figure 2.5) were cut out from an equilibrated system of two palmitic acid monolayers separated by a water slab simulated previously by S. Sláčík [12] so that a 5Å thick layer of water was left hydrating the carboxyl headgroups. Slab of initial aqueous organics solution similar to the one from previous MD simulation (see section 2.3.1 above) was then inserted between the two hydrated monolayers and the newly created slab was centered within the $52 \times 52 \times 300$ Å^3 unit cell, with a vacuum layer above and below in the z direction. The thickness of the aqueous organics solution in the z direction remained 68 Å. In this way, we obtained systems consisting of 232 palmitic acid molecules arranged in two monolayers of 116 palmitic acid molecules per monolayer separated by a slab of aqueous solution containing 20 aromatic solutes and a total of 5977 water molecules for benzoic acid, 5917 for neutral L-phenylalanine and 6381 for zwitterionic L-phenylalanine. Short equilibration (see Computational details) was performed to let the individual subsystem settle together.

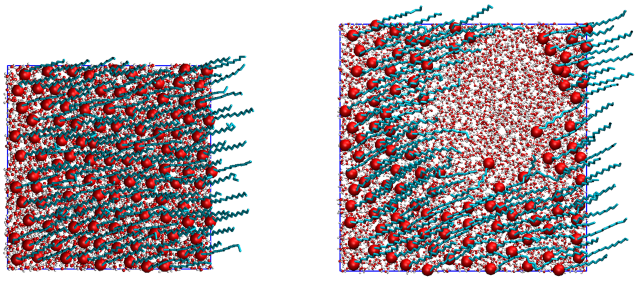

Figure 2.5: Top view of the PA monolayer at the air-water interface for lateral box sizes of 52 Å (left) and 64 Å (right) used in the present simulations. Aliphatic chains are rendered in cyan while carboxylic headgroups are depicted as red beads.

2.3.3 Tilted condensed – 2D gas phase coexistence of palmitic acid monolayer at aqueous organics solution subphase

To create a solution slab with the palmitic acid monolayer configuration mimicking the tilted condensed – 2D gas phase coexistence state at the surface of the solution, the same procedure as described above in section 2.3.2 was employed, using the pre-equilibrated palmitic acid monolayer on water slab from the previously simulated system [12] with the lateral box size of 64 Å (mean area of 35 Å^2/molecule, see Figure 2.5) and the aqueous solution slab of the dimensions of $64 \times 64 \times 68$ Å^3 with 30 molecules of aromatic species. The concentration of organics in the systems remained approximately the same as in section 2.3.1, total of 8996 water molecules was used for benzoic acid aqueous solution, 8921 for neutral L-phenylalanine and 8901 for zwitterionic L-phenylalanine solution. Further simulation details are given below.

2.4 Computational details

For MD equilibration and production runs a double precision version of GROMACS 4.5.5 software [25] was used. Newton's equations of motion

$$\frac{F_i}{m_i} = \frac{\partial^2 r_i}{\partial t^2}, \tag{2.1}$$

where i runs over all atomic coordinates in the system, have been integrated using the "leap-frog" algorithm [29], which calculates positions (equation 2.2) and velocities (equation 2.3) of all particles in every step of the simulation based on relations

$$r(t + \Delta t) = r(t) + v\left(t + \frac{\Delta t}{2}\right)\Delta t \tag{2.2}$$

$$v(t + \frac{\Delta t}{2}) = v\left(t - \frac{\Delta t}{2}\right) + \frac{F(t)}{m}\Delta t, \tag{2.3}$$

and produces trajectories that are identical to the Verlet algorithm [30].

To avoid close contacts between atoms in the initial stages of the simulations, which would cause strong repulsion of the molecules and possibly even a collapse of the simulation due to the high intermolecular forces, each system was initially equilibrated at 100 K using a short time step of 0.5 fs and the velocity rescaling thermostat with a stochastic term [31] (v-rescale) with $\tau_t = 0.1$ ps scaling time constant. This thermostat ensures that a proper canonical ensemble (NVT or NpT) is generated. Initial velocities were generated according to the Maxwell-Boltzmann distribution for temperature of 10 K. In particular, systems prepared by assembling of various fractional subsystems had to be carefully equilibrated to let the subsystems settle together until the total energy was stabilised. Other parameters of the equilibration were identical to those used in the production runs.

For production runs the time step of 2 fs was used to integrate the equations of motion 2.1. Atom coordinates were saved every 1000 propagation steps (i.e. every 2 ps). All bond lengths were constrained using LINCS algorithm (LINear Constraint Solver) [32]. The temperature was maintained at 298 K using the v-rescale thermostat. Control simulations with the Berendsen thermostat [33] were also performed as this thermostat was used in reference [9]. It was confirmed that the choice of thermostat does not have observable influence on the results. Aforementioned conditions correspond to the isochoric-isothermal (NVT) ensemble with constant number of particles, volume and temperature. In some cases, isobaric-isothermal (NpT) simulations with semiisotropic pressure coupling using the Berendsen barostat [33] with the time constant $\tau_p = 1$ ps were performed to compress the box laterally depending on the chosen value of the pressure in the x and y direction (0.5 bar, 1.0 bar, 1.5 bar, 10 bar or 100 bar), while pressure in the z direction was kept at zero.

The evaluation of the forces (derivatives of the interaction potential) demands most of the CPU time. It is common practice in classical MD simulations to use several approaches, such as the constrained intramolecular motions

(LINCS) and the truncation of the intermolecular potential, to save computational resources and/or reach longer simulation times while preserving desirable accuracy. The effect of the electrostatic interactions have been accounted for by the fast smooth particle-mesh Ewald (PME) method [34] decomposing the Coulomb potential into short range and long range contributions, which are treated separately. A 1nm cutoff distance for both the Lennard-Jones potential and the short range part of the Ewald sum was used while the reciprocal part of the Ewald sum was treated by quickly convergent summation in the Fourier space with a grid spacing of 0.12 nm and a fourth-order interpolation.

2.5 Trajectory analysis

Positions and velocities of all atoms are stored every 1000 propagation steps in a compressed trajectory file (*.tpr) for further analysis. Visual inspection of the trajectories can be carried out by a visualisation software, in our case VMD [27, 28]. For quantitative analysis, GROMACS software comes with a set of analysis tools for trajectory and energy files (*.edr). Specifically, the utilities g_energy, g_density, g_rdf and g_order were used [26]. The groups of atoms of a certain type, used by these programs in the analysis procedures, are specified by the user in the atom index files (*.ndx).

G_energy provides time evolution of macroscopic system properties over a selected section of the simulation - energy, temperature, pressure, density, box dimensions and volume, etc., and was primarily used to monitor the equilibration of the systems.

G_density calculates the mass density profiles by the following procedure. The slab is divided into 300 equal slices in the direction perpendicular to the palmitic acid monolayer - water interface and the partial density of the selected subsystem (defined in the index file) in each slice is averaged over a selected section of the simulation time. The mean density of the subsystem is then plotted as the function of z coordinate in a given accuracy, determined by the number of slices, the slab dimensions and the time window. The mass density profiles were normalized to the maximum density.

The radial distribution function (RDF) describes how the density (or, equivalently, probability of finding) of the particle of type B varies as a function of distance from a reference particle of type A. The function is defined by formula

$$g_{AB}(r) = \frac{1}{\langle \rho_B \rangle} \frac{1}{N_A} \sum_{i \in A}^{N_A} \sum_{j \in B}^{N_B} \frac{\delta(r_{ij} - r)}{4\pi r^2}, \tag{2.4}$$

where the normalization factor $\langle \rho_B \rangle$ stands for the mean density of the particles of type B and $N_{A/B}$ is the total number of the particles of type A or B. In practice the g_rdf program calculates $\langle \rho_B \rangle$ as the B particles density averaged over all spheres surrounding the particles A with the radius equal to the half of the smallest of the box dimensions. The system is divided into spherical layers (from r to $r + dr$) and the δ-function in (2.4) is approximated by a histogram, averaged over the selected time interval of the simulation.

Due to the slab configuration of the systems studied here (i.e., in addition to the system itself also vacuum layer is present in the simulation box), $\langle \rho_B \rangle$

improperly reproduces the bulk density, which leads to the incorrectly normalized RDFs. For the quantitative comparison of the various investigated system, therefore, the running coordination number is used. It is directly calculated from the radial distribution functions as

$$n_{AB}(R) = 4\pi \int_0^R g_{AB}(r) r^2 \, \mathrm{d}r, \tag{2.5}$$

providing information about the mean number of the B particles present within the sphere of radius R surrounding the reference atom of type A.

The order parameter S_z calculated by g_order is correlated with the molecular organization in the system. In our particular case of the palmitic acid monolayer deposited on an aqueous organics solution, we investigate the average spatial orientation along the aliphatic chains. The order parameter is defined as

$$S_z = \frac{1}{2}\langle 3\cos^2\theta_n - 1\rangle, \tag{2.6}$$

where θ_n is the instantaneous angle between the segmental vector linking C(n-1) and C(n+1) atoms of the hydrocarbon chain and the surface normal. S_z can range from a value of -1/2 (orientation perpendicular to the surface normal) to 1 (orientation parallel to the surface normal).

In addition to the above quantities, the tilt angle and dihedral angle distributions for palmitic acid were calculated using Python scripts kindly provided by Lukasz Cwiklik. Tilt angle of an individual palmitic acid molecule is calculated as the angle of the vector defined by the C1 (COOH headgroup) and C16 (terminal CH_3 group) atoms with respect to the z-axis averaged over a selected section of the trajectory. A dihedral angle is defined by four neighboring carbon atoms A, B, C, D of the palmitic acid aliphatic chain as the angle between the planes ABC and BCD.

Regardless of the particular initial configuration used for the NVT ensemble simulations, we observed stabilization of the equilibrium between the adsorption of the aromatic species to the headgroup region of the palmitic acid monolayer and their bulk concentration in aqueous solution no later than after 20 ns. The first 20 ns of each simulation was therefore discarded and the rest of the trajectory was used for analysis. The equilibration was monitored by the time-resolved density profiles calculated over 5ns time windows of the trajectory and the system was considered equilibrated when the bulk density of the aromatic species remained identical for the consecutive intervals.

3. Results and discussion

By performing the simulations of the molecular dynamics on the systems described in the previous chapter we aim to answer the questions stated in the introductory part of the thesis. This is done by the visual inspection of the system dynamics as well as by means of the trajectory analysis. The following structural parameters were calculated - density profiles of the systems, radial distribution functions, dihedral angles of the headgroup region of the palmitic acid, and the tilt angles and order parameters of the palmitic acid hydrocarbon chains.

In the figure legends throughout this chapter, the various parts of the systems are labelled as follows - palmitic acid molecules 'pa', benzoic acid molecules 'ba' and L-phenylalanine molecules 'phe'. The abbreviations given in capital letters refer to atom names (see Appendix B for the schematic depiction of the molecules with atom names and numbering). Please note that the C1 atom of the benzoic acid molecule is denoted as CZ in Figures 3.1-3.5 for easier comparison with L-phenylalanine.

3.1 Surface of aqueous organics solution

The systems of aqueous organics solution, described in Section 2.3.1, were simulated under NVT ensemble conditions, the total production simulation time with the benzoic acid was 50 ns, for the neutral and zwitterionic L-phenylalanine molecules it was 100 ns. All aromatic species exhibit surface activity and their adsorption to the solution surface occurs during the initial phases of the simulation. As seen from the time-resolved snapshots (see Appendix C), once the aromatics reach the air-aqueous interface (after about 600 ps) and the mean concentration of the aromatics in the surface layer and in the aqueous phase is stabilized, the aromatic molecules remain predominantly at the surface and occasionally diffuse back to the aqueous phase. The decrease in the bulk concentration of the benzoic acid in the aqueous phase is not unphysical as the initial concentration (0.20 mol/l) used in the system was well above the experimentally observed solubility (0.025 mol/l). However, for the zwitterionic L-phenylalanine, the initial concentration of which (0.18 mol/l) corresponded to its solubility, the bulk concentration stabilizes below the experimental one, indicating that more L-phenylalanine molecules would need to be supplied into the system to reach a saturated solution phase in equilibrium with the surface-adsorbed L-phenylalanine molecules. In contrast to the zwitterion, the initial concentration of the neutral L-phenylalanine corresponded to an unphysical state as the existence of the neutral form of L-phenylalanine in the aqueous environment at neutral pH is marginal. Therefore, the forcing of the neutral L-phenylalanine out of the solution, observed in the simulation, is expected.

The density profiles plotted in Figure 3.1 were computed over 30 ns interval (from 20 ns to 50 ns of the trajectory) for the benzoic acid aqueous solution and over 80 ns interval (from 20 ns to 100 ns of the trajectory) for the L-phenylalanine aqueous solutions with 0.1 nm resolution along the z axis and renormalized so that the maximum value is equal to 1. The systems of the benzoic acid and the

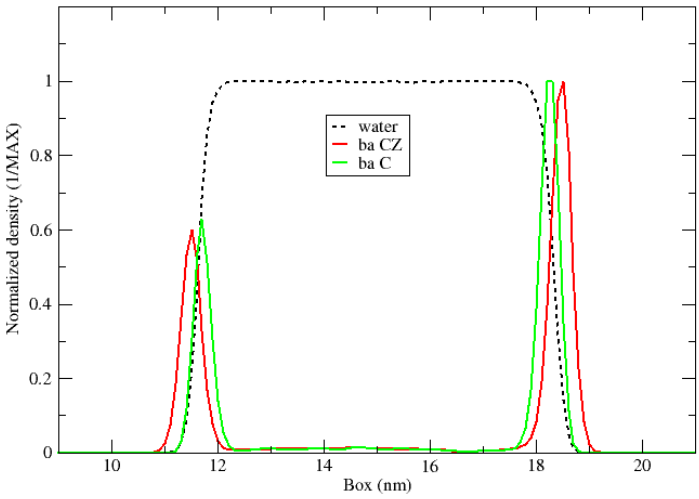

(a) Benzoic acid

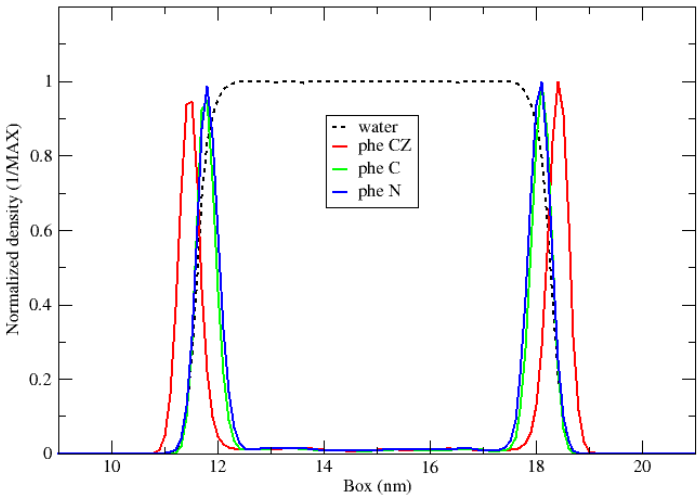

(b) Neutral L-phenylalanine

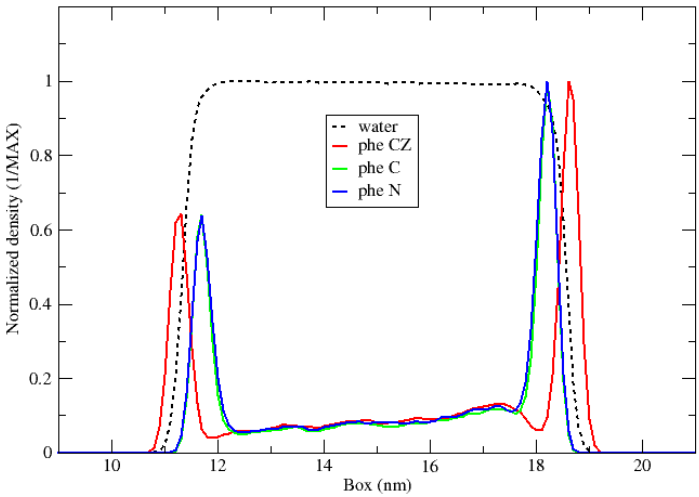

(c) Zwitterionic L-phenylalanine

Figure 3.1: Density profiles for the systems of the aqueous organics solution

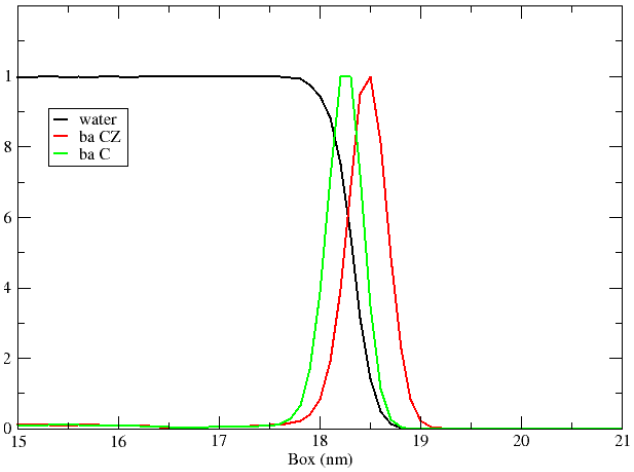

(a) Benzoic acid

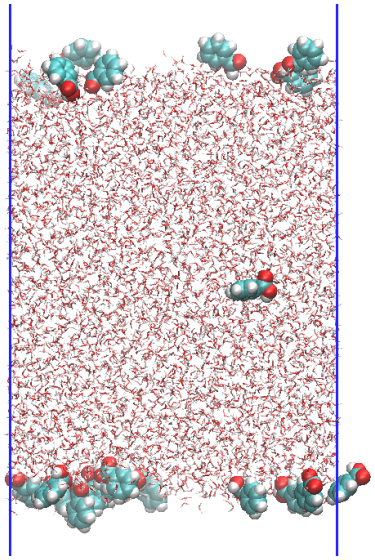

(b) Final configuration

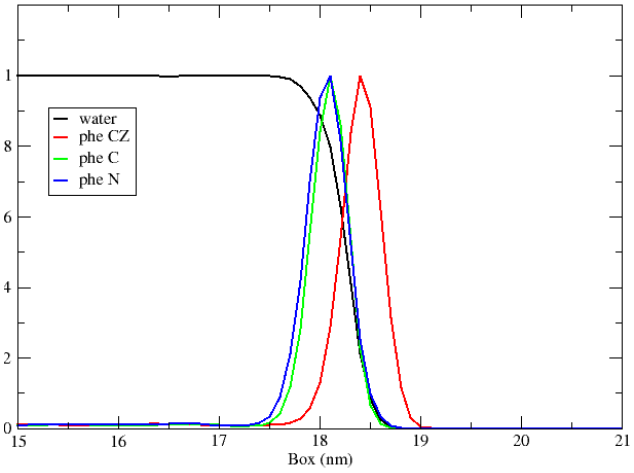

(c) Neutral L-phenylalanine

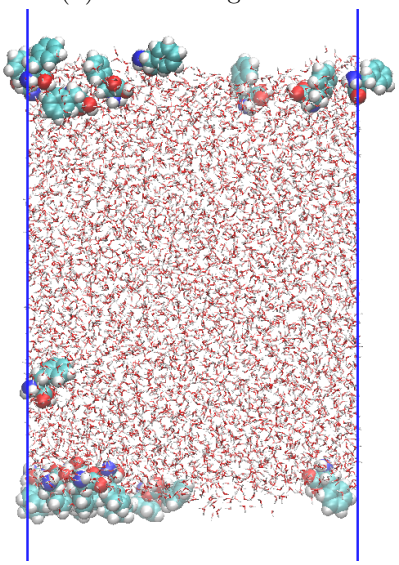

(d) Final configuration

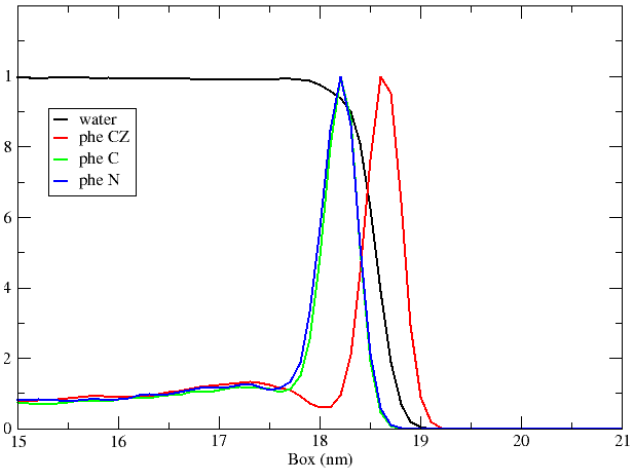

(e) Zwitterionic L-phenylalanine

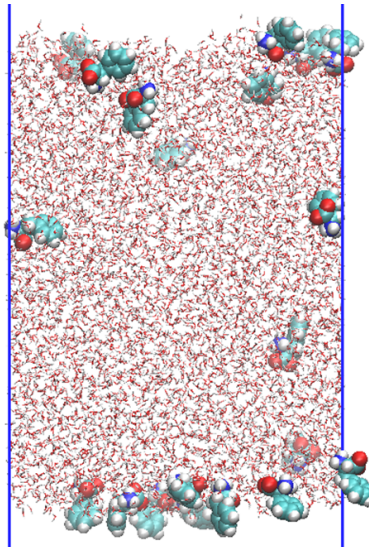

(f) Final configuration

Figure 3.2: Detail of the density profiles of the air-aqueous interface

zwitterionic L-phenylalanine are not well equilibrated in terms of the same concentration of the aromatic species at both of the air-aqueous interfaces. This is caused by the initial random, uneven distribution of the organic molecules between the two surfaces in the first 20 ns of the simulations and their relatively long surface residence times which hinder the redistribution of the molecules from one interface to the other. This feature of the systems can be remedied by the appropriate prolonging of the simulation time which was not necessary for our purposes as we are primarily interested in the orientation of the organic molecules at the surface. From the detailed zoom of the density profiles in the region of the air-aqueous interface showed in Figure 3.2 we can conclude that the orientation of the aromatic molecules at the surface is such that the hydrophilic groups of the aromatic species are predominantly solvated, with the amino and carboxyl groups pointing to the aqueous phase. The visual inspection of the trajectories showed that the aromatic ring lies at the water surface or points to the gas phase depending on how deeply is the molecule immersed in water.

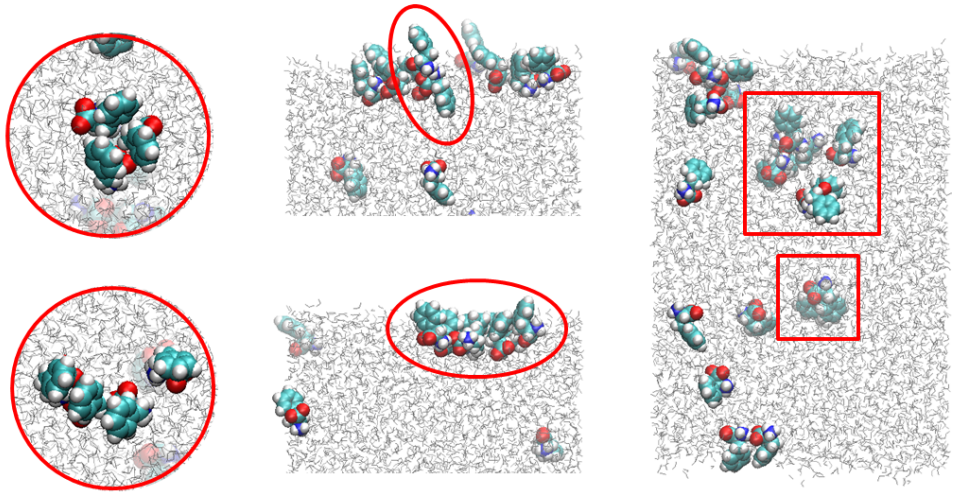

Figure 3.3: Zwitterionic L-phenylalanine clusters at the surface (red circle) and in the bulk (red square). From left to right, from top to bottom - typical trimer, linear trimer, phenyl ring pointing to the aqueous solution due to interaction with the molecule at the surface, preferred orientation of the molecules in the large cluster at the surface and various bulk clusters.

In addition to the above discussed uneven distribution of benzoic acid and L-phenylalanine molecules between the two interfaces, the density profile of the aqueous zwitterionic L-phenylalanine solution shows that the bulk density is not constant across the aqueous slab; rather, the L-phenylalanine concentration is higher in the subsurface region of one of the interfaces compared to the other one. Moreover, this character of the density curve dos not change over the time of the simulation (confirmed by the comparison of the density profiles calculated over 15ns time intervals). This may be indicative of the presence of L-phenylalanine clusters at and below the surface. Indeed, by the visual inspection of the simulation we can observe the formation of the clusters at the surface as well as in the bulk. A substantial part of the clusters present in the interfacial region is partially immersed in the aqueous solution so that the polar headgroups of the

zwitterions are interacting together, leading to the phenyl rings of some of the molecules forming the cluster pointing into the aqueous phase. In contrast, the clusters of benzoic acid and neutral L-phenylalanine are predominantly formed right at the surface, with the phenyl rings either lying flat on water or pointing into the gas phase.

Clusters of the aromatic species (Figure 3.3) in the bulk and at the surface are mostly formed as dimers, which decompose very quickly, and trimers, which are more stable. The typical structure of the trimers is such that two molecules are π-π stacked and the third molecule stabilizes this conformation. Also other conformations were observed, e.g. the linear and bended linear arrangement based on π-π (dispersion interactions) and polar headgroup-headgroup interactions (by hydrogen bonding and salt bridges), however, they are less common. Larger clusters occur mainly in the air-aqueous interface. The largest observed cluster consisted of 9 molecules.

In summary, the MD simulations of the aqueous organics solution in the slab configuration confirmed the surface activity (propensity of the molecules for the air–aqueous interface) of the investigated aromatic species. The simulations also yielded molecular-level details regarding the preferential orientation of the surface-adsorbed molecules, namely that their polar headgroups remain well hydrated, whereas the more hydrophobic aromatic moieties point into the gas phase. In addition, the simulations revealed a rather strong tendency for the molecules to aggregate, in particular at the aqueous-air interface. The observed structures of the aggregates suggest that the clusters are stabilized by both headgroup-headgroup interactions as well as by π-π stacking of the aromatic rings.

3.2 Tilted condensed phase of palmitic acid monolayer at aqueous organics solution subphase

The systems containing two palmitic acid monolayers with the mean molecular area of 23 Å^2/molecule separated by the aqueous organics solution slab described in Section 2.3.2, were simulated under NVT ensemble conditions for the total of 50 ns (see Appendix C for the time-resolved snapshots). Following the results of the MD simulations performed by Griffith et al. [9] on the stearic acid monolayers (21 Å^2/molecule) at aqueous benzoic acid solution, we expected the benzoic acid molecules in our system to intercalate into the palmitic acid film in a similar manner. The authors of the study observed during the 50ns MD simulation the plunging of the benzoic acid phenyl ring into the monolayer, causing the occurrence of the regions lacking in the surfactant coverage and thus allowing the bulk molecules easily access the surfactant film regardless of the compressed state of the monolayer.

Despite the use of the fatty acid with a shorter chain length (palmitic acid instead of stearic acid) and the monolayer with a lower density (a mean area of 23 Å^2/molecule), both of which should make the intercalation of foreign molecules easier, we did not observe such event for either of the aromatic species at this timescale. It suggests that the behaviour of the aromatic species at the palmitic

acid-aqueous interface strongly depends on the chosen force field [36], as the GROMOS force field was used for the parametrization of the stearic acid by Griffith et al. [9] while we used the OPLS force field for the palmitic acid (the same force field was used for benzoic acid in both cases). The two fatty acid force fields differ most of all in the parametrization of the carboxyl headgroup. In addition to somewhat different Lennard-Jones parameters, the main difference concerns the charge distribution, with the OPLS charges on the COOH atoms being significantly larger than the GROMOS ones, making the carboxyl headgroups of our palmitic acid monolayer markedly more polar compared to the stearic acid simulations of Griffith et al. The use of the different force fields for the aromatic species (GROMOS for benzoic acid, OPLS for neutral and zwitterionic L-phenylalanine) seems not to have a significant influence as none of them intercalate into the palmitic acid monolayer. For further details see Appendix B.

The partitioning of the oxidized aromatics between the solution-monolayer interface and bulk aqueous solution is shown in the density profiles computed over 30 ns interval (from 20 ns to 50 ns of the trajectory) with 0.1 nm resolution along the z axis (Figures 3.4 and 3.4). All density profiles were renormalized by the respective maxima. The mean density of the aromatic species at both of the palmitic acid-aqueous interfaces is not equal because of the same reasons as mentioned above. Once the dynamic equilibrium between the aromatic species in the bulk and those adsorbed to the palmitic acid monolayers is stabilized, we can see the propensity of the zwitterionic L-phenylalanine molecules to stay adsorbed to the monolayer they reached first while the adsorbed benzoic acid and neutral L-phenylalanine molecules migrate between the aqueous phase and the palmitic acid-aqueous interface. The density profiles clearly show that the presence of the amino group in the L-phenylalanine cause the change in the preferential orientation of the molecules towards the monolayer. When adsorbed at the interface, the benzoic acid molecules partially insert their hydrophobic aromatic ring into the palmitic acid film while the hydrophilic carboxyl headgroup remains hydrated. In contrast to the benzoic acid, the neutral and zwitterionic L-phenylalanine molecules orient their hydrophobic part towards the aqueous phase and the amino group towards the palmitic acid headgroups, while the carboxyl group also remains hydrated.

As in the previous simulations of aqueous organics solution slabs with a bare surface, aggregation of the aromatics was observed also here. The formation and decomposition of the clusters is very dynamic. In the bulk, the clusters consisting of maximum four molecules of the aromatic species are formed and the larger clusters occur only at the palmitic acid-aqueous interface. Here, the clusters tent to locally bend the monolayer so that the palmitic acid headgroup region is rippled and some of the palmitic acid headgroups are pressed above or, on the contrary, below other molecules' headgroups. However, despite these perturbations to the monolayer caused by the adsorbed aromatics, the tight packing of the palmitic acid molecules corresponding to the tilted condensed phase of the monolayer remains unchanged, confining the aromatics to the solution-palmitic acid headgroup interfacial region. Intercalation of neither of the aromatics deep into the palmitic acid monolayer, between the hydrocarbon chains of the fatty acids, was not observed.

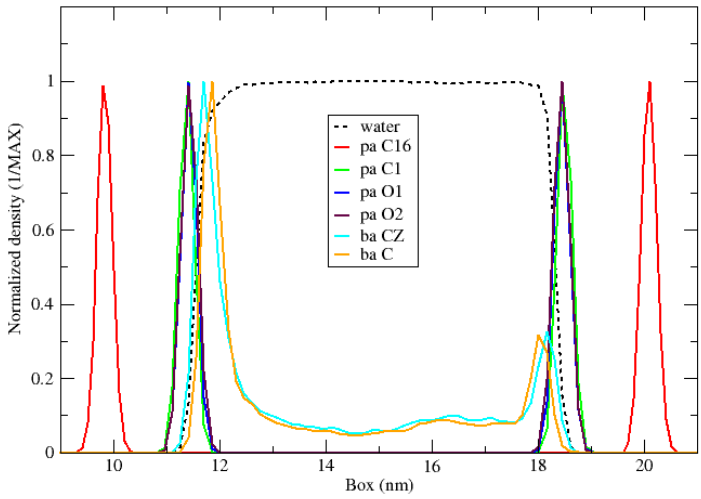

(a) Benzoic acid

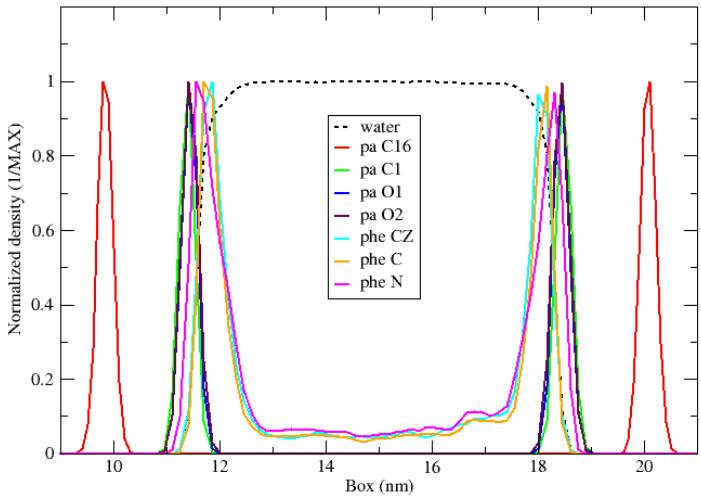

(b) Neutral L-phenylalanine

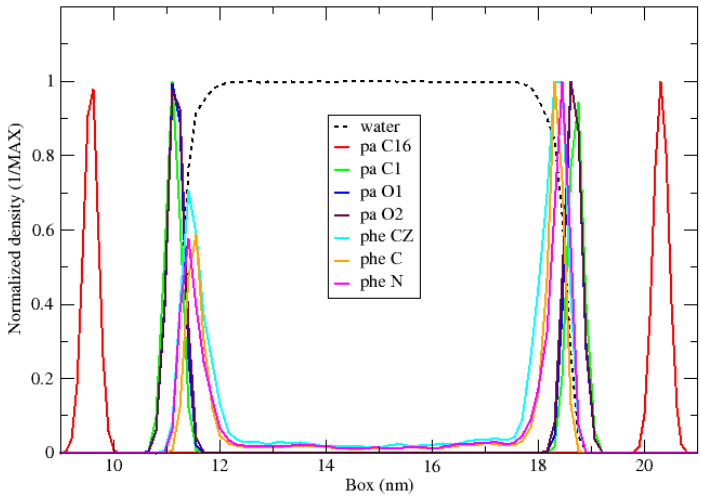

(c) Zwitterionic L-phenylalanine

Figure 3.4: Density profiles for the systems of the tilted condensed phase of palmitic acid monolayer at the aqueous organics solution

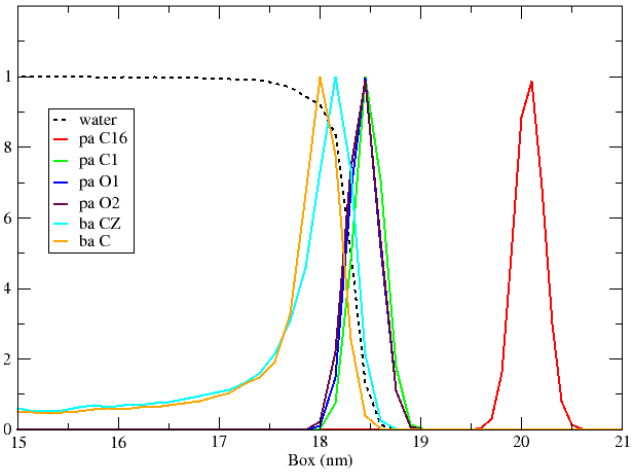

(a) Benzoic acid

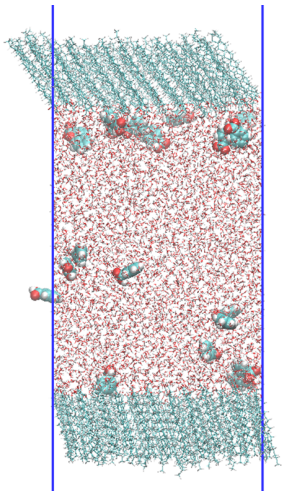

(b) Final configuration

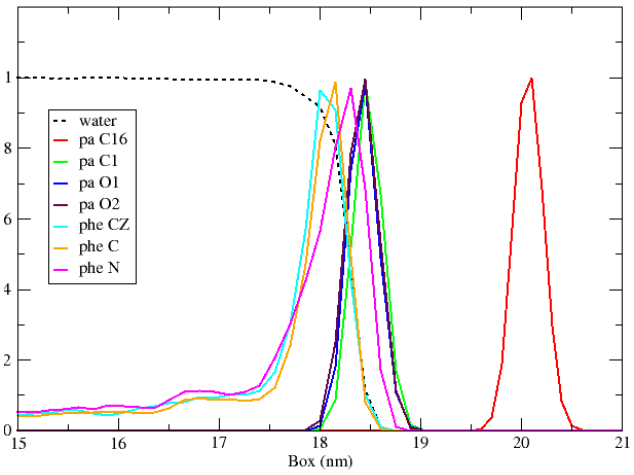

(c) Neutral L-phenylalanine

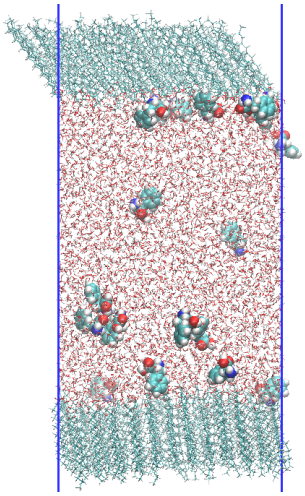

(d) Final configuration

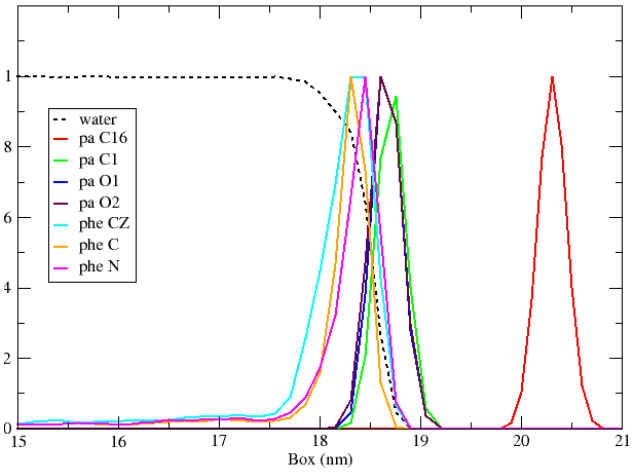

(e) Zwitterionic L-phenylalanine

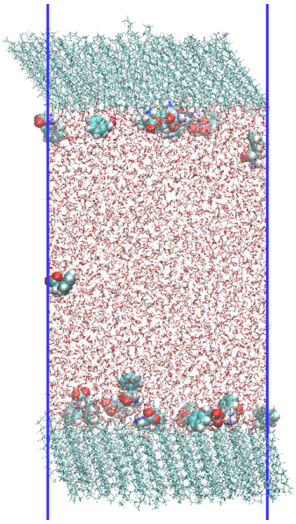

(f) Final configuration

Figure 3.5: Detail of the density profiles of the palmitic acid-aqueous interface

To evaluate the effect of the adsorbed aromatic species onto the palmitic acid monolayer, several structural properties were computed. The distributions of tilt angles of the palmitic acid chains with respect to the interface normal (see Section 2.5), plotted in Figure 3.6, were calculated in the presence and the absence of aromatic species in the system, separately for each of the two monolayers (denoted as 'up' and 'down') in order to capture the influence of the adsorbed molecules as they are distributed unevenly between the two slab surfaces. However, the analysis showed that the tilt angle distributions are practically independent of the adsorbed aromatic molecules and are almost identical. The mean observed value of the tilt angle of the palmitic acid monolayer at water 28.9 ° with full width at half maximum of 7.3 ° is in good agreement with the tilt angle calculated by Plazzer and coworkers [36] on the similar system of an octadecanol monolayer at 23 Å^2/molecule using the OPLS force field.

The dihedral angle distributions for the two neighbouring atom groups, O2-C1-C2-C3 (Figure 3.7, O2 is the oxygen atom of the OH part of the carboxyl headgroup) and C1-C2-C3-C4 (Figure 3.8), provide the information about the preferred conformation of the palmitic acid chain in the headgroup region. The dihedral angles of the central peak around 180 ° represent the trans conformation, while angle values lower than 120 ° or higher than 240 ° correspond to the gauche conformation. The monolayer at 23 Å^2/molecule is closely packed, which leads to the straightening of the chains and makes the trans conformation dominating in both distributions. The O2-C1-C2-C3 dihedral angle can be also viewed as the measure of the rotational freedom of the headgroup and the C1-C2-C3-C4 dihedral angle distribution is also correlated with the immersion depth of the palmitic acid chains in the aqueous subphase. The molecules deeper in the water tend to occur in the gauche conformation. The aromatic species adsorbed to the palmitic acid-aqueous interface induce small decrease of the trans conformation population in comparison with the system of the palmitic acid monolayer at the water.

The order parameter S_z (see equation (2.6)) of the palmitic acid monolayer, indicating a degree of order along the aliphatic chain, is plotted in Figure reffig:order as a function of carbon atom position starting from the carboxyl headgroup. To investigate the influence of the adsorbed aromatic species on the order parameter, we compared the analysis performed at each of the monolayers (denoted as 'up' and 'down') with the average order parameter of the palmitic acid monolayer deposited on the pure water. All of the order parameter curves agree well with the trend observed for the monolayer of the eicosanoic acid at water for 23 Å^2/molecule, studied by McMullen and Kelty [37]. As in the case of the eicosanoic acid monolayer, we have also found that S_z is smaller in the middle of the chains and increases near the headgroup and at the end of the chains, dropping significantly again for the terminal carbon atom. For all of the systems studies, the adsorbed aromatic species increase somewhat the order of the palmitic acid chains near the carboxyl headgroup in comparison with the case of the palmitic acid at the pure water. The order of the chains further inside the monolayer is not influenced by a direct contact with the aromatics, as they did not penetrate beyond the headgroup region.

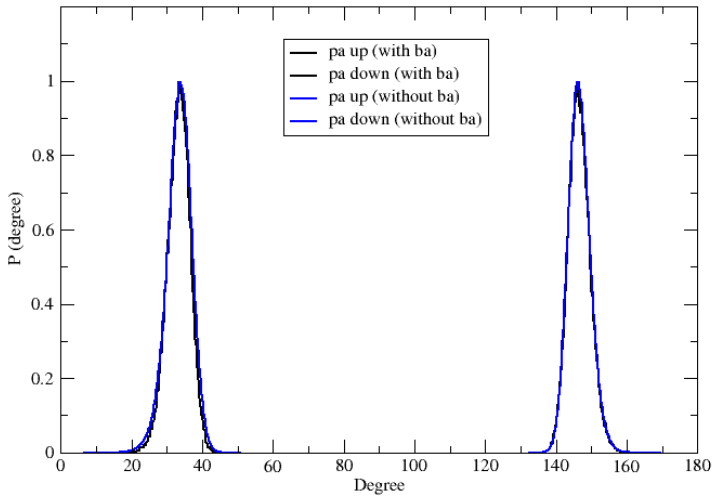

(a) Benzoic acid

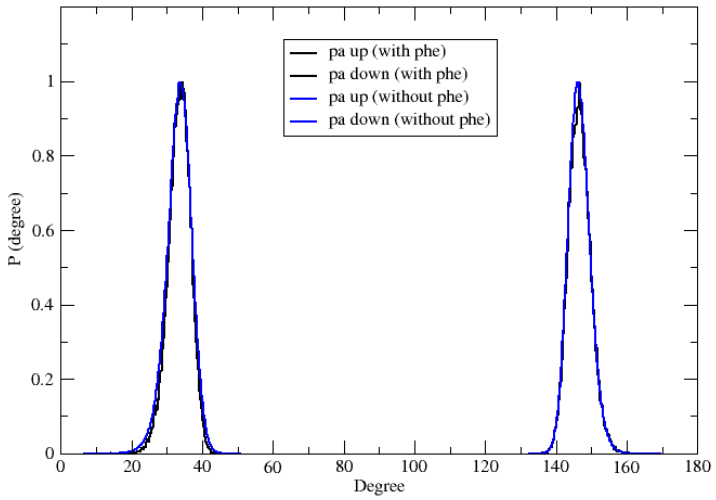

(b) Neutral L-phenylalanine

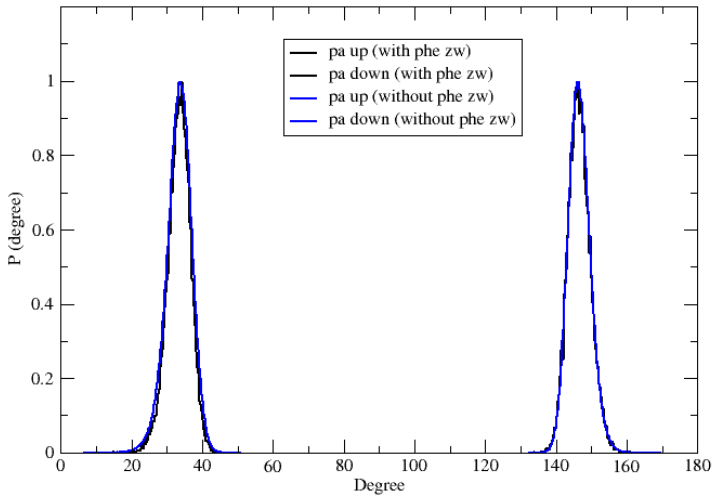

(c) Zwitterionic L-phenylalanine

Figure 3.6: Palmitic acid chain tilt angle distributions at 23 Å^2/molecule in the presence and the absence of the aromatic species in the system

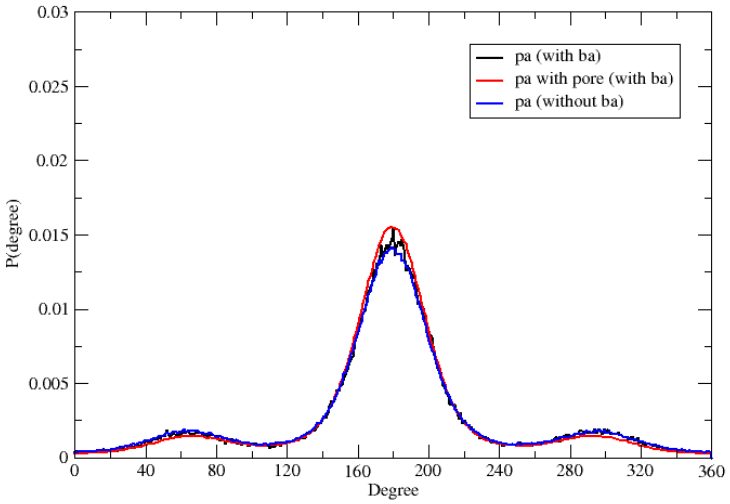

(a) Benzoic acid

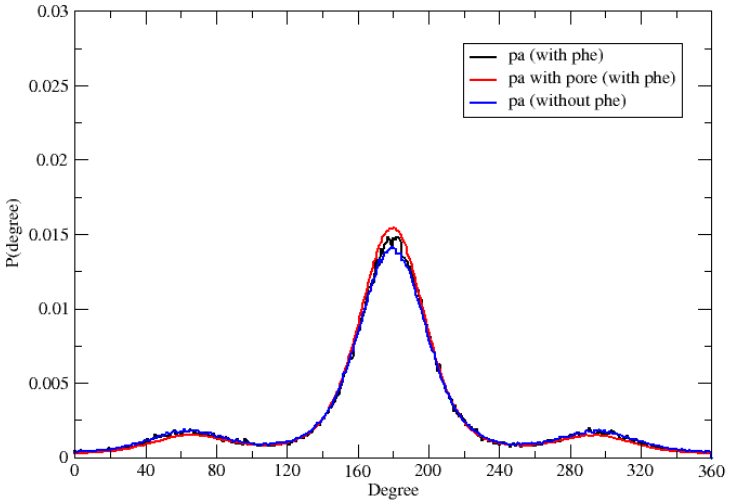

(b) Neutral L-phenylalanine

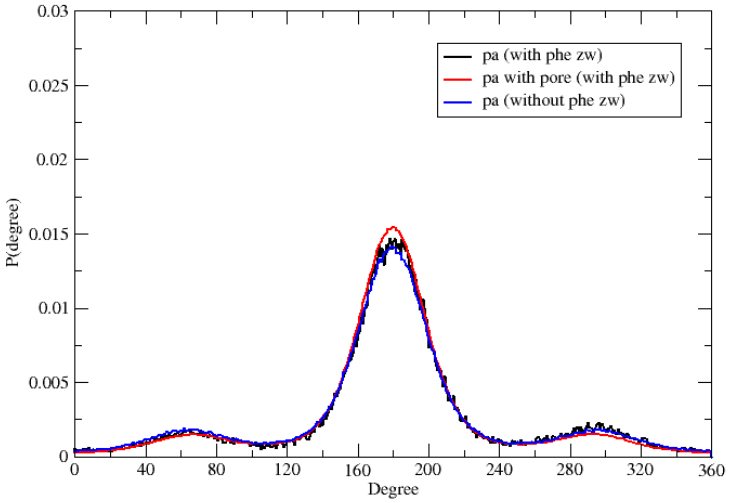

(c) Zwitterionic L-phenylalanine

Figure 3.7: Palmitic acid O2-C1-C2-C3 dihedral angle distributions in the presence and the absence of the aromatic species in the system

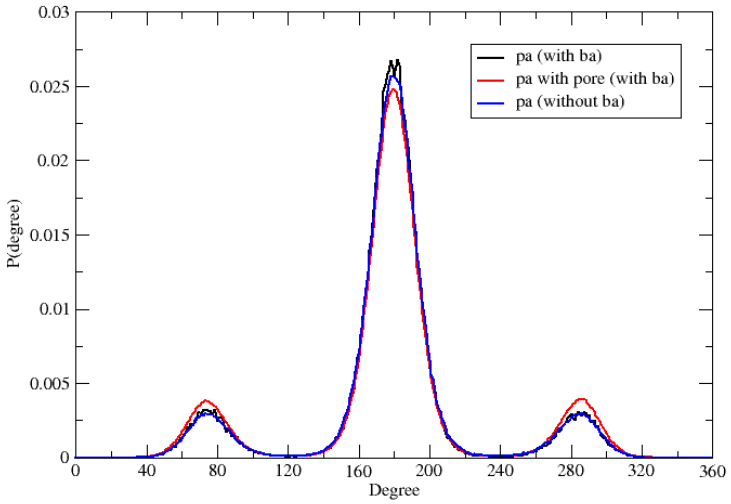

(a) Benzoic acid

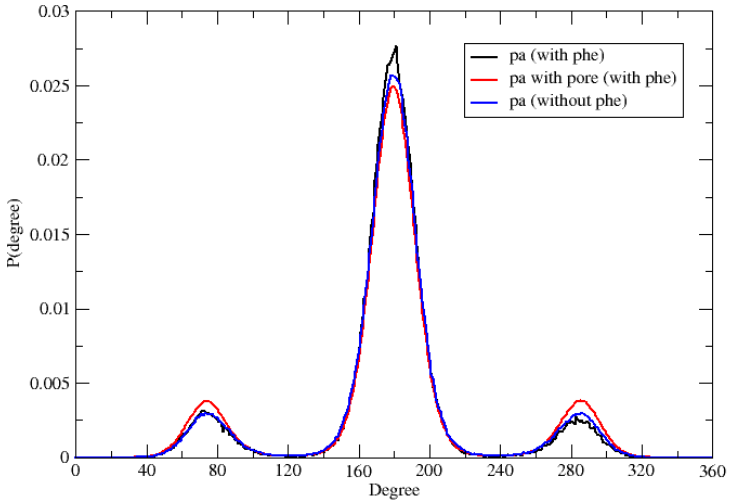

(b) Neutral L-phenylalanine

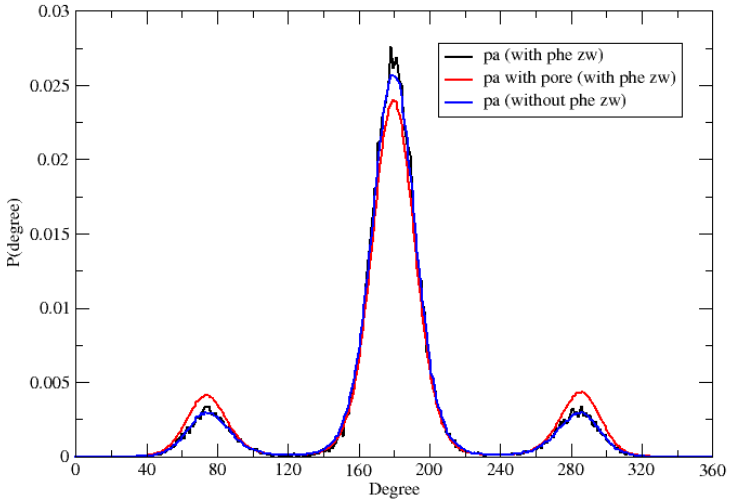

(c) Zwitterionic L-phenylalanine

Figure 3.8: Palmitic acid C1-C2-C3-C4 dihedral angle distributions in the presence and the absence of the aromatic species in the system

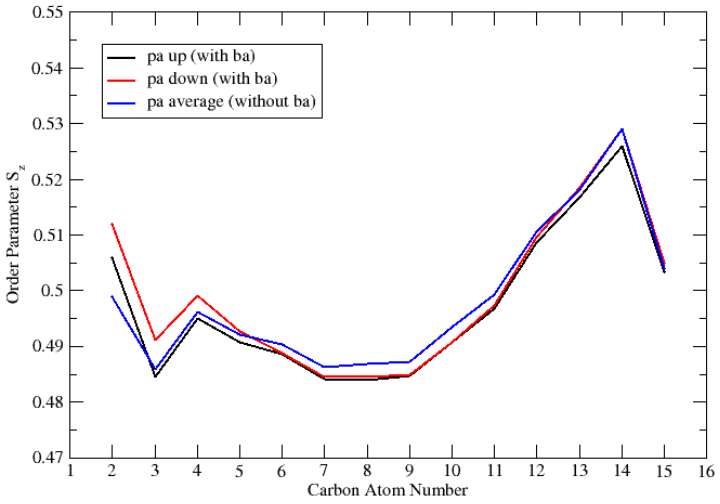

(a) Benzoic acid

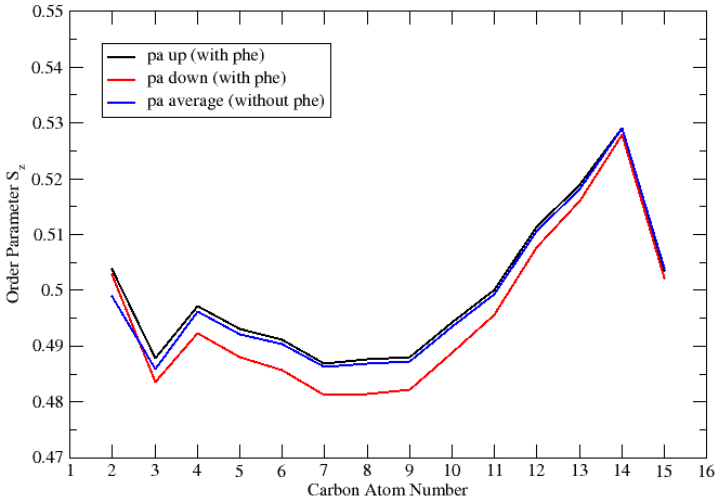

(b) Neutral L-phenylalanine

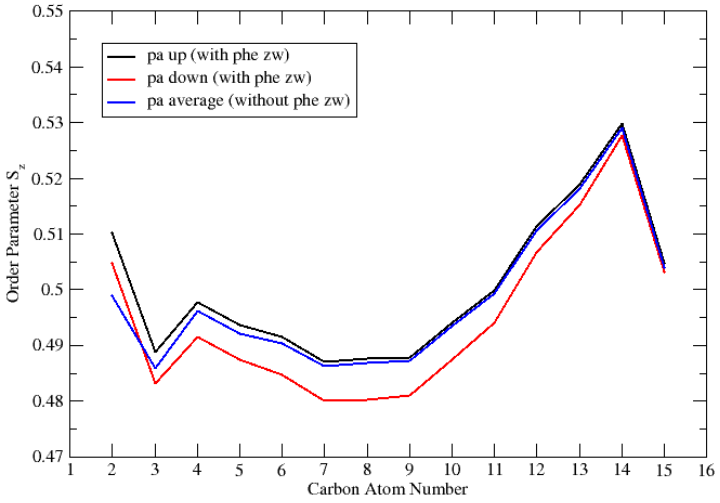

(c) Zwitterionic L-phenylalanine

Figure 3.9: Order parameters of the palmitic acid monolayers in the tilted condensed phase at the aqueous organics solution

3.3 Tilted condensed – 2D gas phase coexistence of palmitic acid monolayer at aqueous organics solution subphase

The simulations of the tilted condensed – 2D gas phase of palmitic acid monolayer at the aqueous organics solution aimed at mimicking the adsorption process of L-phenylalanine to the solution-monolayer interface in the experimental system in the "fully open barrier position" of the Langmuir trough [9]. The systems were simulated under NVT ensemble conditions for the total of 50 ns. The mean molecular area of the palmitic acid film deposited on the aqueous organics solution subphase was 35 $Å^2$/molecule. At this mean density, a "pore" is present in the monolayer (i.e., a roughly circular region of uncovered aqueous surface), while the palmitic acid molecules covering the rest of the surface adopt a tilted condensed arrangement with a mean area per molecule approximately 28 $Å^2$ (see Section 2.3.3).

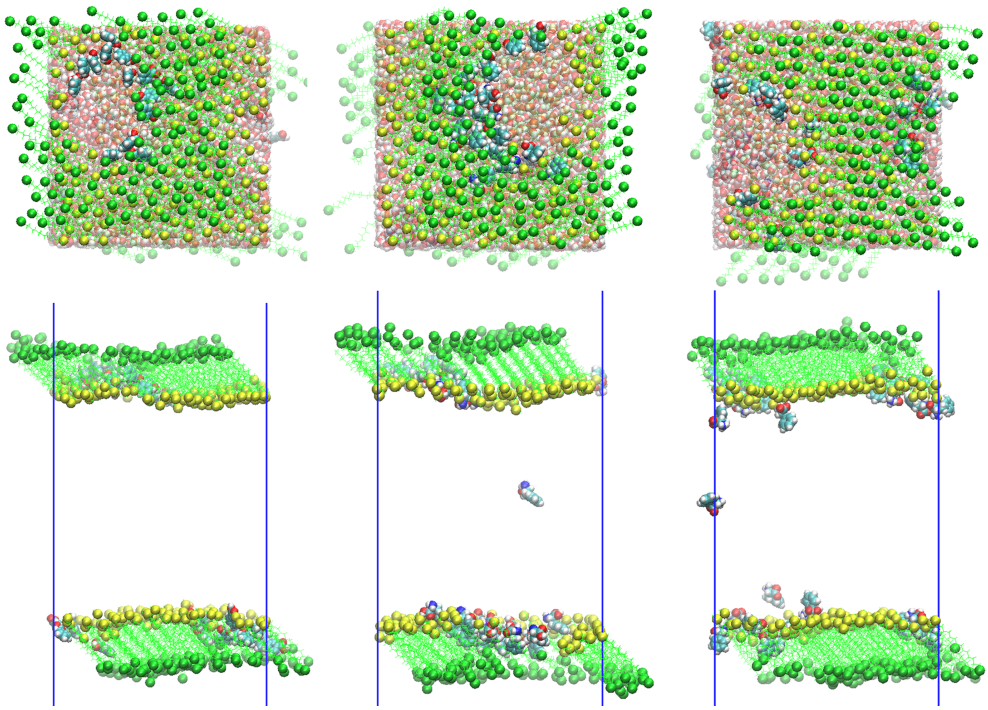

Figure 3.10: Final configurations of the NVT simulations of the palmitic acid in the tilted condensed – 2D gas phase at the aqueous organics solution subphase, the lateral (bottom) and top view, from left to right - benzoic acid, neutral and zwitterionic L-phenylalanine systems.

The final configurations of the systems are depicted in Figure 3.10. The aromatic molecules from the aqueous solution adsorb to the interface, strongly preferring the bare aqueous surface, particularly the edge of the pore on the side where the palmitic acid molecules are tilted towards the free aqueous phase. In this wedge-like space, the molecules take advantage of the most favourable balance of various interactions. As elsewhere within the free portion of the interface, they have the possibility to adopt a favourable orientation with their polar headgroups

hydrated and their phenyl rings pointing away from water. Here, however, they have additional stabilization due to the interaction with the tilted hydrophobic hydrocarbon chains of the palmitic acid molecules. The preference of the aromatic molecules for this confined space leads to their substantial aggregation. The orientation of the molecules in the clusters present on the air-aqueous interface is the same as observed for the pure aqueous organics solution. The orientation of the molecules closest to the edge of the pore is not uniform, because it depends also on the molecules present in the surrounding. The molecules that remain adsorbed below the monolayer, interacting with the palmitic acid headgroups, behave similarly to those in the tilted condensed phase palmitic acid monolayer system. We can visually observe the propensity of the benzoic acid and neutral L-phenylalanine molecules to stay adsorbed to the edge of the monolayer they reached as the first while the zwitterionic L-phenylalanine molecules diffuse also back to the aqueous phase.

For the film density corresponding to a mean area of 35 $Å^2$/molecule, after the pore occurs, the palmitic acid chains in the monolayer covering the rest of the aqueous surface are still closely packed (at the mean area per molecule of approx. 28 $Å^2$) which leads to the preservation of the ratio between trans and gauche conformation populations in the O2-C1-C2-C3 and C1-C2-C3-C4 dihedral angle distributions observed for the film density of 23 $Å^2$/molecule (see Figures 3.7 and 3.8 above in Section 3.2). The population of the gauche conformation is little smaller for the O2-C1-C2-C3 and higher for the C1-C2-C3-C4 dihedral angle compared to 23$Å^2$/molecule dense film. The change is obviously caused by the presence of the edge of the monolayer in the system.

The order parameter S_z (see equation (2.6)) of the palmitic acid monolayer is plotted in Figure 3.11 as a function of carbon atom position starting from the carboxyl headgroup. In comparison with the analysis performed in previous section (see Figure 3.9) for the tilted condensed phase of palmitic acid monolayer (without a void present) at the aqueous organics solutions of the same concentration, the values of the order parameters of the palmitic acid in the tilted condensed – 2D gas phase are lower. This lowering of the overall order is due to the lower density of the palmitic film with the void present (mean molecular area of 28$Å^2$/molecule compared to 23$Å^2$/molecule in the previous system without the void). The increase of the order of the upper half of the chains (from the carbon atom #8) with respect to the central region of the hydrocarbon chains is somewhat less pronounced than in the previous case, what can be caused by the free space available for the chains surrounding the void while the rest of the hydrocarbon chains are still held together by the hydrophobic interactions. While the order parameter curves for the monolayers on the upper and lower surfaces agree well with each other for both neutral and zwitterionic L-phenylalanine, for benzoic acid they are shifted significantly with respect to each other (although they both exhibit the same trends). We note, however, that in all three systems the aromatic molecules are distributed approximately equally between the two interfaces. As the S_z strongly depends on the palmitic acid film density, it can be indicative of the change in film density due to the different structure of the benzoic acid aggregates adsorbed to the edge of the pores on the upper vs. the lower interface.

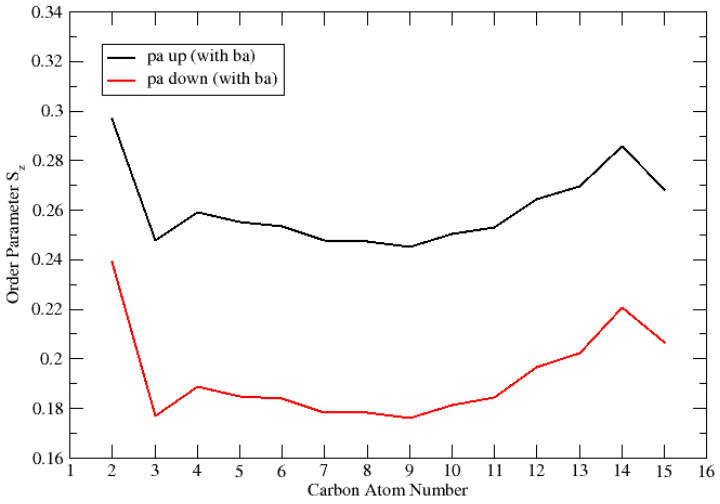

(a) Benzoic acid

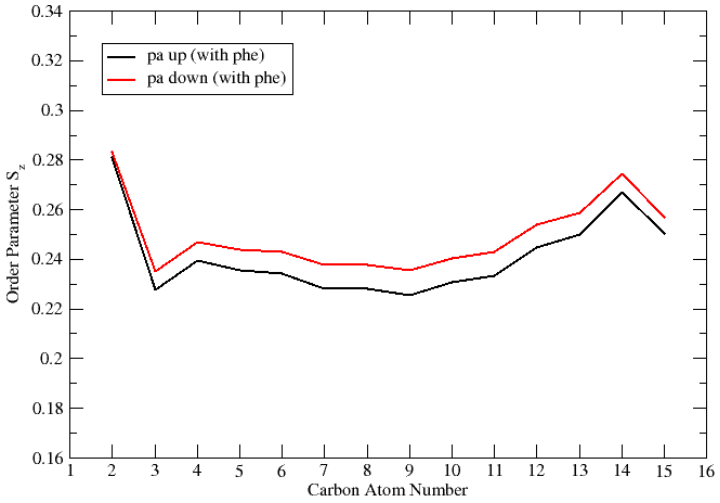

(b) Neutral L-phenylalanine

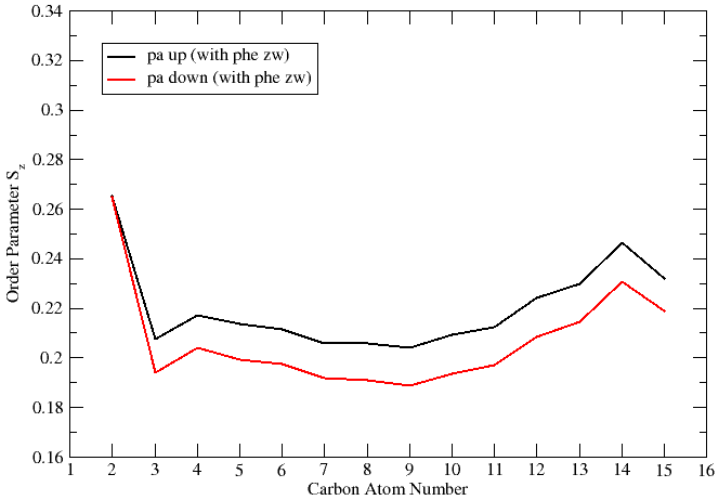

(c) Zwitterionic L-phenylalanine

Figure 3.11: Order parameters of the palmitic acid monolayers in the tilted condensed – 2D gas phase at the aqueous organics solution

3.4 Compression simulations

Starting from the final configuration of the previous NVT simulation of the solution slab with the palmitic acid monolayer in the tilted condensed - 2D gas phase coexistence state, NpT simulation was performed to mimic a typical Langmuir trough compression experiment once the water-soluble aromatic molecules were allowed to adsorb to the interface [9, 10]. While it would be interesting to do this simulation for benzoic acid as well as for both forms of L-phenylalanine, it was performed only for the neutral L-phenylalanine due to the lack of time.

The use of the several different values of the lateral pressure (0.5 bar, 1.0 bar and 1.5 bar) in the 20ns control simulations showed that the choice of the pressure value (within the above range) influences only the speed with which the simulated system is laterally compressed, however, the final configurations were quite similar for all three values of the lateral pressure. Therefore, the first 20ns of the production simulation were performed at 1.5 bar. To achieve further compression of the palmitic acid monolayer, this initial compression stage was followed by another 20ns simulation at 10 bar bar, and finally the simulation was allowed to proceed for a total of 200 ns at 100 bar. The lateral box dimensions gradually compressed from initial 64 Å to 47 Å, leading to the mean surface area per palmitic acid molecule decrease from 35 $Å^2$ to 19 $Å^2$. It is important to note that the real surface density of the film is higher as the part of the surface is occupied by the L-phenylalanine molecules. The evolution of the MD simulation within the first few nanoseconds is depicted in the Figure **??**.

Within the first 7 ns of the simulation at 1.5 bar, the L-phenylalanine molecules adsorbed to the edge of the monolayer pore are "pushed" gradually by the palmitic acid molecules towards the centre of the contracting pore and finally forced to form a cluster filling the space between the palmitic acid molecules of the closing "walls" of the pore, across the full depth of the monolayer. An important questions, which the MD simulations can help to answer, is whether the aromatics will be forced to dissolve back into the aqueous phase, stay in the pore or will be squeezed out of the monolayer to the palmitic acid-air interface with the increasing pressure. As the compression proceeds at 10 bar and subsequently at 100 bar, after approximately 110 ns of the total simulation time the equilibrium between the adsorbed aromatic molecules and those in the bulk aqueous solution is reached. The L-phenylalanine molecules freely diffuse from the cluster-aqueous interface to the aqueous phase and back.

The clusters in the pores of the monolayer formed during the initial stages of the compression (at 1.5 bar and then at 10 bar), such as the one shown in the top left snapshot of Figure 3.13 do not show any significant ordering. The various cluster structures seen in the first and second row of Figure 3.13 are present during the 100bar compression phase. The L-phenylalanine molecules at the borders of the clusters exposed to the air preferentially point out by their aromatic ring as the hydrophilic headgroups which provide stronger interaction are involved in the binding of the cluster. The highly ordered clusters, as seen in the third row of Figure 3.13, are formed in the second half of the 100bar compression simulation. The continued pressure from the monolayer forces the molecules in the pore to arrange themselves very tightly in a cylindrical like shape with the aromatic rings in the outer shell - the molecules in the chains normal to the monolayer are bonded

by the headgroup-headgroup interactions (COOH...NH_2 hydrogen bonds) and π-π stacking interactions, and the cluster in the monolayer is held by the dispersion interactions between the hydrophobic parts of the palmitic acid (hydrocarbon chain) and L-phenylalanine molecules (aromatic ring). The plane of the aromatic ring tents to orient close to parallel alignment with the hydrocarbon chains of the palmitic acid molecules in the monolayer, however, in many cases only tilted orientation is possible.

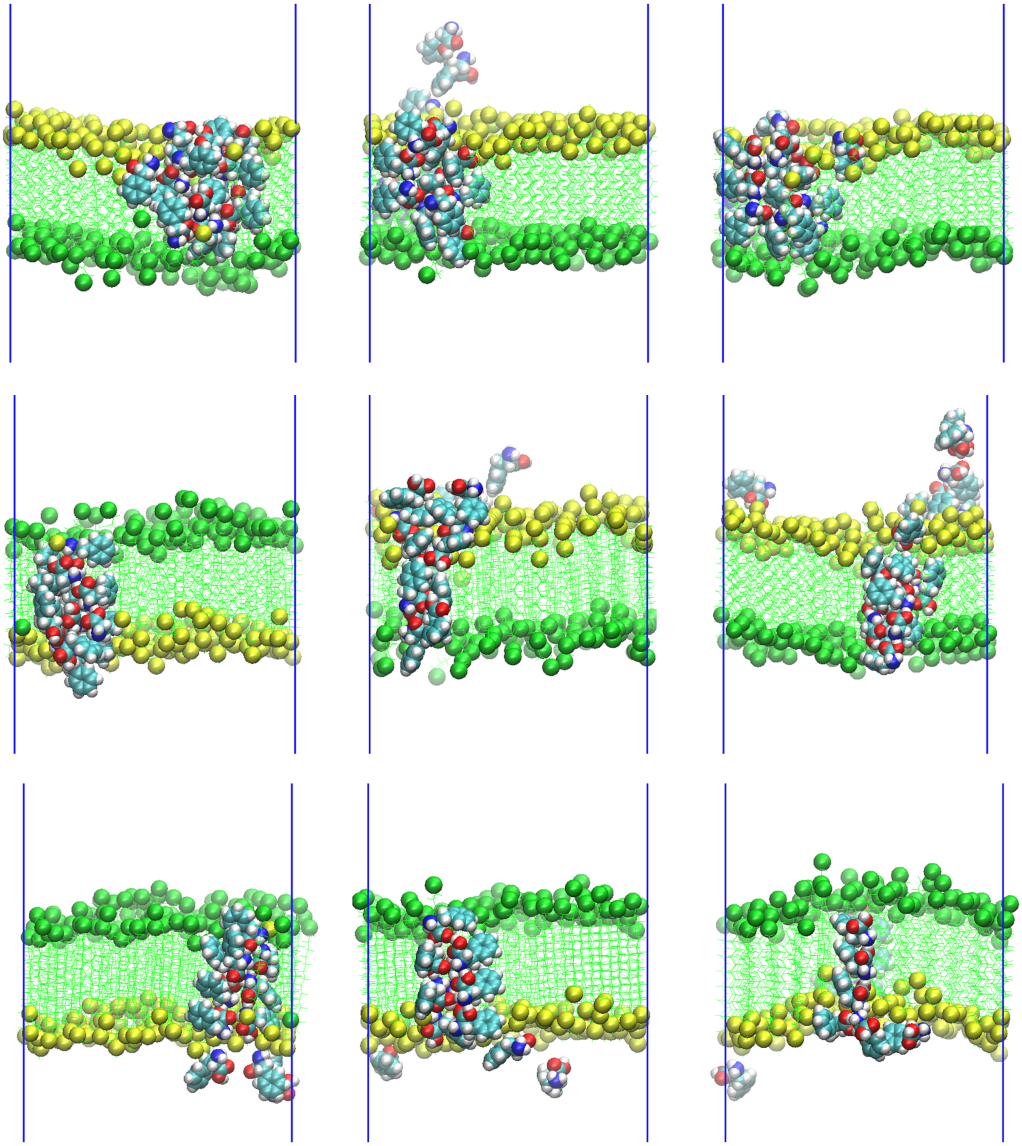

Figure 3.13: Clusters of the neutral L-phenylalanine molecules caught in the pore. The aliphatic chains of the palmitic acid molecules are rendered in green, the terminal C16 atoms are shown as green beads while carboxylic headgroups as yellow beads, the water molecules below the palmitic acid-aqueous interface (yellow beads) are not shown.

During the simulation, we observed few events of the water molecule uptake from the aqueous phase into the pore by the hydrophilic headgroup of the L-phenylalanine (see Figure 3.14). However, with the increased pressure, the water molecules were squeezed out of the cluster and pushed back to the aqueous phase.

No evaporation of the water molecules enhanced by the presence of the monolayer pore filled by the L-phenylalanine molecules was observed.

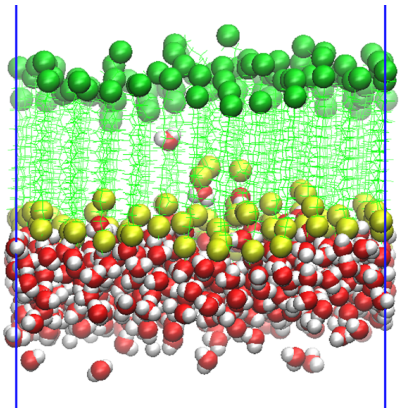

Figure 3.14: Water molecule uptake. The aliphatic chains of the palmitic acid molecules are rendered in green, the terminal C16 atoms are shown as green beads while carboxylic headgroups as yellow beads.

The visual inspection of the simulations revealed that the palmitic acid molecules in the vicinity of L-phenylalanine are also affected by the L-phenylalanine cluster formation. Two such cases are shown in Figure 3.15. In the first one (Figure 3.15, left), the headgroup of a palmitic acid molecule was "pulled" into the hydrophobic part of the monolayer by a L-phenylalanine headgroup, forcing the palmitic acid molecule to bend into a "hairpin" conformation. In the course of time, however, the palmitic acid molecule returned to the normal orientation through mutual shifts of the palmitic acid chains and the motion of the L-phenylalanine molecules in the cluster. In the second case, the palmitic acid molecule was initially pushed out of the monolayer, to the palmitic acid-air interface, where it lay on top of the palmitic acid monolayer for some time and then inserted back into the monolayer "end first", leaving the COOH headgroup in between the terminal methyl groups of the other palmitic acid molecules (Figure 3.15, middle). So it remained until the end of the simulation (Figure 3.15, right).

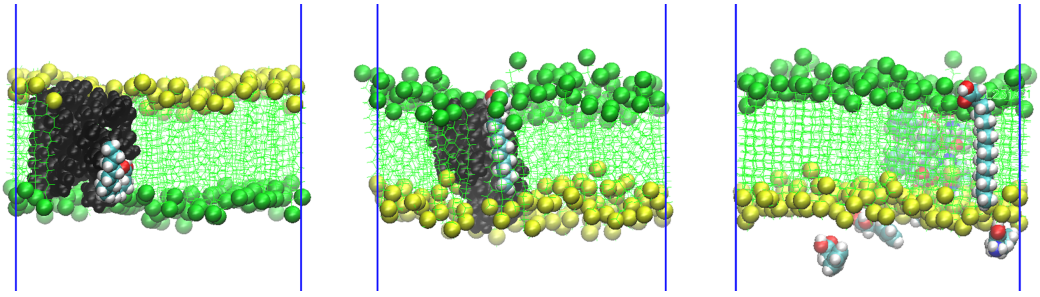

Figure 3.15: Disordered palmitic acid molecules in the monolayer. Clusters of the L-phenylalanine molecules caught in the pore are rendered in black and the aliphatic chains of the palmitic acid molecules in green color, the terminal C16 atoms are shown as green beads while carboxylic headgroups as yellow beads, the water molecules below the palmitic acid-aqueous interface (yellow beads) are not shown.

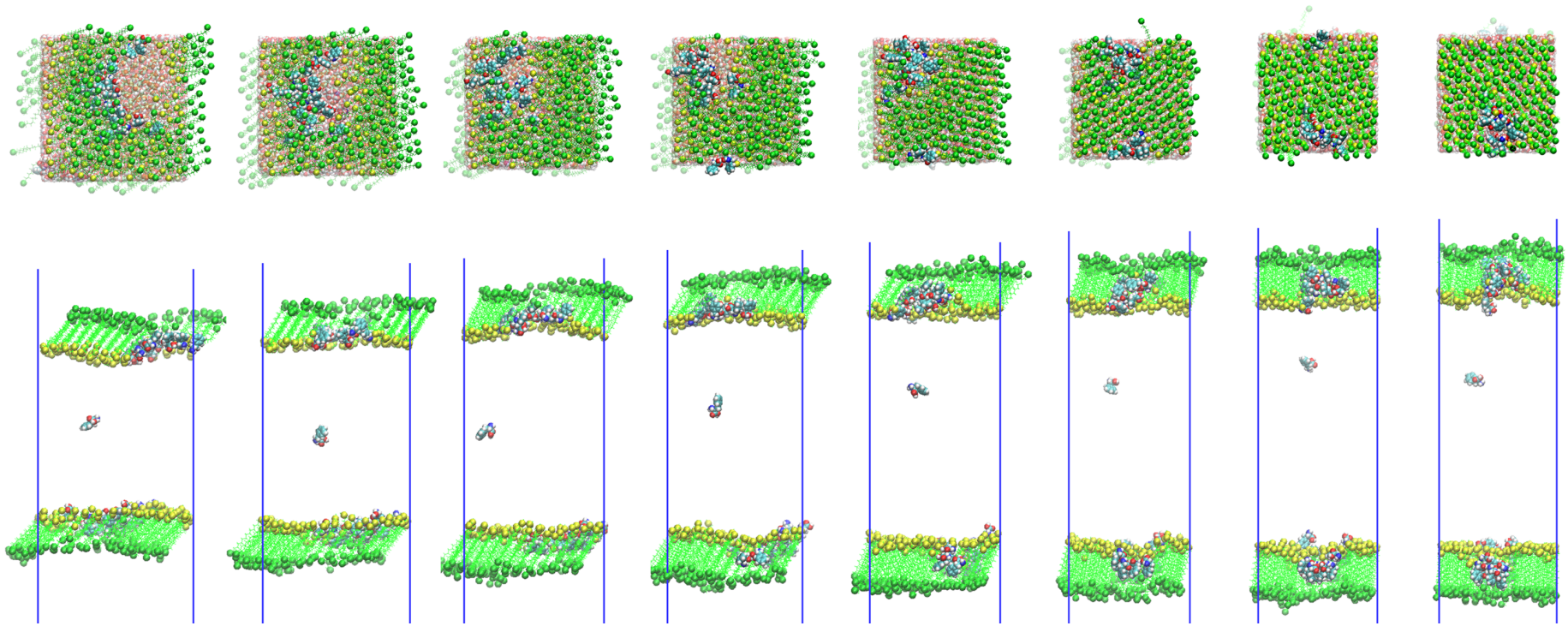

Figure 3.12: Compression of the L-phenylalanine aqueous solution slab with the palmitic acid monolayer in the tilted condensed - 2D gas phase coexistence state. The aliphatic chains of the palmitic acid molecules are rendered in green, the terminal C16 atoms are shown as green beads while carboxylic headgroups as yellow beads, the water molecules between the two surfaces are not shown.

4. Conclusions

The goal of this study was to perform and analyse molecular dynamics simulations of aqueous solutions of selected organic aromatic species (benzoic acid, neutral and zwitterionic L-phenylalanine), both with and without palmitic acid monolayer present at the solution-air interface. The work aims at answering the questions given in the Introduction section of this thesis, and providing molecular-level insight into the findings of recent experimental studies of mixed aromatic-aliphatic surfactant films [9, 10].

The main results of this thesis can be summarised as follows:

1. The selected empirical model (combination of force fields) is able to reproduce the experimentally observed surface activity of both benzoic acid and L-phenylalanine.

2. The partitioning of the oxidized aromatics at the air-aqueous interface coated with a palmitic acid film was investigated. For the palmitic acid film in the tilted condensed phase fully coating the aqueous-air interface, the aromatic molecules exhibited propensity for adsorption to the headgroup region of the palmitic acid monolayer, however, they were not observed to intercalate into the monolayer. In the case mimicking the tilted condensed - 2D gas phase coexistence state of the palmitic acid monolayer, the aromatics strongly preferred adsorption to the free solution surface at the border with the tilted palmitic acid molecules.

3. The simulation of the palmitic acid monolayer on the benzoic acid aqueous solution which was carried out for comparison with the results published in the literature showed a strong dependence of the behaviour of the aromatic species at the fatty acid-aqueous interface on the force field used to parametrize the fatty acid molecules. The OPLS force field used in our calculation does not reproduce the spontaneous intercalation of the BA into the fatty acid monolayer reported in reference [9].

4. The molecular-level details regarding the preferential orientation of the molecules adsorbed to the surface of the aqueous organics solution and palmitic acid-aqueous interface was provided.

5. The simulations revealed a rather strong tendency for the aromatic molecules to aggregate, in particular at the air-aqueous and palmitic acid-aqueous interface. The observed structures of the aggregates suggest that the clusters are stabilized by both headgroup-headgroup interactions as well as by π-π stacking of the aromatic rings.

6. The analysis of the tilt and dihedral angles distributions of the palmitic acid Langmuir monolayers did not show significant change in these quantities caused by the adsorption of the aromatic species in the headgroup region of palmitic acid within the computational accuracy.

7. The compact palmitic acid monolayer in the tilted condensed state (the film density of 23 Å^2/molecule) at the aqueous organics solution is resistant to the water evaporation on the timescale of the simulations ($\sim$ 100 ns).

8. In the compression simulation, the water molecule uptake was observed during the formation of the L-phenylalanine cluster in the pore of the palmitic acid monolayer. However, the water evaporation throughout the cluster was not observed.

9. The cluster of the L-phenylalanine molecules filling the pore in the palmitic acid monolayer was found to exhibit a highly ordered structure based on headgroup-headgroup interactions and π-π stacking under the increased lateral pressure of 100 bar.

5. Appendices

5.1 Appendix A - Interaction potential

Mutual interaction of atoms moving at a potential energy surface is described in classical MD simulations by expansion of the potential into a set of bonding (intramolecular) and non-bonding (intermolecular) contributions to the overall interaction. Depending on the features of the model system we want to capture, the series can be truncated at the pairwise additive terms or, on the contrary, further augmented by many-body terms. Coefficients of these empirical potentials (force fields) are usually fitted to ab-initio data or experimentally obtained thermodynamical properties like density, vaporization enthalpy, melting temperature etc.

In a simple forcefield like OPLS used in our simulations, the electrostatic interaction between two point charges q_1 and q_2 at a distance r is given by Coulomb law

$$V_C(r) = \frac{1}{4\pi\epsilon_0}\frac{q_1 q_2}{r}, \tag{5.1}$$

where ϵ_0 is electric permitivity of a vacuum. The short range repulsive and long range attractive van der Waals interaction are empirically described by the Lennard-Jones potential [35], most commonly written as

$$V_{LJ}(r) = 4\epsilon\left[\left(\frac{\sigma}{r}\right)^{12} - \left(\frac{\sigma}{r}\right)^{6}\right] = \frac{A}{r^{12}} - \frac{B}{r^{6}}, \tag{5.2}$$

where constants ϵ and σ depend on the types of the two interacting atoms and represent the depth of the potential well and the distance in which the potential has a zero value, respectively. Some of the forcefields' parametrizations (e.g. GROMOS forcefield) instead use constants A and B. For easy comparison, we have converted them into ϵ and σ based on the relations $A = 4\epsilon\sigma^{12}$ and $B = 4\epsilon\sigma^{6}$. Since only parameters for pairs of identical atom types are given in the OPLS library [26], others are derived via mixing rules

$$\begin{aligned} \epsilon_{ij} &= \sqrt{\epsilon_{ii}\epsilon_{jj}} \\ \sigma_{ij} &= \sqrt{\sigma_{ii}\sigma_{jj}}. \end{aligned} \tag{5.3}$$

As regards the bonding interactions, stretching of a chemical bond between a pair of atoms is approximated by the harmonic potential

$$V_b(r) = \frac{1}{2}k_b\left(r - r_0\right)^2 \tag{5.4}$$

with k_b being a force constant determining the strength (rigidity) of the bond and $(r - r_0)$ a displacement from the optimal bond length r_0. At this level, effects like anharmonic vibrations and bond dissociation cannot be described. The same harmonic form is used for valence angle vibrations

$$V_a(\theta) = \frac{1}{2}k_a\left(\theta - \theta_0\right)^2. \tag{5.5}$$

Here k_a stands for the force constant and θ_0 for the equilibrium angle between three bonded atoms. The most important interaction determining different molecular conformations is given by torsion (dihedral) angle potential, usually described by first few term of even Fourier series

$$V_d(\phi) = \sum_d k_d \left[\cos(d\phi - \phi_0)\right], \tag{5.6}$$

where k_d is the force constant and ϕ_0 is the equilibrium angle between the planes ABC and BCD defined by four bonded atoms A, B, C and D.

5.2 Appendix B - Force field parameters

Table 5.1: Atom types, corresponding atomic charges and Lennard-Jones parameters of the SPC/E model of water

Atom	Atom type	Partial charge [e]	ϵ [kcal]	σ [Å]
OW	OW	-0.8476	0.6502	0.3166
HW1	HW	0.4238	0	0
HW2	HW	0.4238	0	0

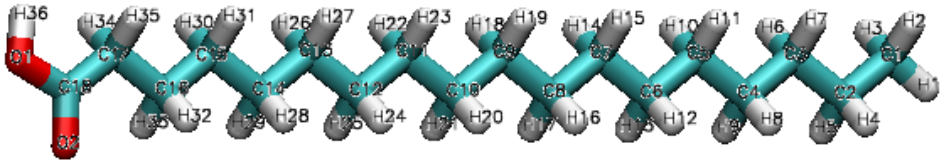

Figure 5.1: Stearic acid molecule with atom names and numbers

Table 5.2: Atom types and corresponding parameters of the GROMOS96 54a7 force field with atomic charges and charge groups (separated by horizontal lines) used for the stearic acid molecule in reference MD simulation [9]

Atom	Atom type	Partial charge [e]	ϵ [kcal]	σ [Å]
C18	C	0.354	0.2774	0.3581
O2	O	−0.332	1.2791	0.2760
O1	OA	−0.268	0.8496	0.2955
H36	H	0.197	0	0
C17	C	−0.134	0.2774	0.3581
H35	HC	0.079	0.1184	0.2373
H34	HC	0.079	0.1184	0.2373
C16	C	−0.091	0.2774	0.3581
H33	HC	0.058	0.1184	0.2373
H32	HC	0.058	0.1184	0.2373
C15	C	−0.106	0.2774	0.3581
H31	HC	0.054	0.1184	0.2373
H30	HC	0.054	0.1184	0.2373
C14	C	−0.106	0.2774	0.3581
H29	HC	0.053	0.1184	0.2373
H28	HC	0.053	0.1184	0.2373
C13	C	−0.106	0.2774	0.3581
H27	HC	0.052	0.1184	0.2373
H26	HC	0.052	0.1184	0.2373
C12	C	−0.104	0.2774	0.3581
H25	HC	0.052	0.1184	0.2373
H24	HC	0.052	0.1184	0.2373
C11	C	−0.103	0.2774	0.3581
H23	HC	0.052	0.1184	0.2373
H22	HC	0.052	0.1184	0.2373
C10	C	−0.103	0.2774	0.3581
H21	HC	0.051	0.1184	0.2373
H20	HC	0.051	0.1184	0.2373

continues on the next page

Atom	Atom type	Partial charge [e]	ϵ [kcal]	σ [Å]
C9	C	−0.102	0.2774	0.3581
H19	HC	0.051	0.1184	0.2373
H18	HC	0.051	0.1184	0.2373
C8	C	−0.102	0.2774	0.3581
H17	HC	0.051	0.1184	0.2373
H16	HC	0.051	0.1184	0.2373
C7	C	−0.102	0.2774	0.3581
H15	HC	0.051	0.1184	0.2373
H14	HC	0.051	0.1184	0.2373
C6	C	−0.102	0.2774	0.3581
H13	HC	0.051	0.1184	0.2373
H12	HC	0.051	0.1184	0.2373
C5	C	−0.102	0.2774	0.3581
H11	HC	0.051	0.1184	0.2373
H10	HC	0.051	0.1184	0.2373
C4	C	−0.102	0.2774	0.3581
H9	HC	0.051	0.1184	0.2373
H8	HC	0.051	0.1184	0.2373
C3	C	−0.104	0.2774	0.3581
H7	HC	0.051	0.1184	0.2373
H6	HC	0.051	0.1184	0.2373
C2	C	−0.1	0.2774	0.3581
H5	HC	0.049	0.1184	0.2373
H4	HC	0.049	0.1184	0.2373
C1	C	−0.11	0.2774	0.3581
H3	HC	0.038	0.1184	0.2373
H2	HC	0.038	0.1184	0.2373
H1	HC	0.038	0.1184	0.2373

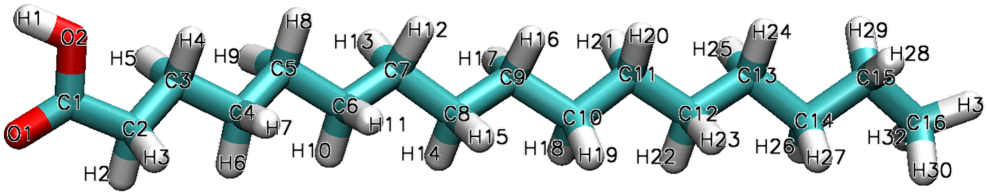

Figure 5.2: Palmitic acid molecule with atom names and numbers

Table 5.3: Atom types and corresponding parameters of the OPLS force field with atomic charges and charge groups (separated by horizontal lines) used to parametrize the palmitic acid molecule

Atom	Atom type	Partial charge [e]	ϵ [kcal]	σ [Å]
C1	C	0.52	0.4393	0.3750
O1	O_3	−0.44	0.8786	0.2960
O2	OH	−0.53	0.7113	0.3000
H1	HO	0.45	0	0
C2	CT	−0.12	0.2761	0.3500
H2	HC	0.06	0.1255	0.2500
H3	HC	0.06	0.1255	0.2500
C3	CT	−0.12	0.2761	0.3500
H4	HC	0.06	0.1255	0.2500
H5	HC	0.06	0.1255	0.2500
C4	CT	−0.12	0.2761	0.3500
H6	HC	0.06	0.1255	0.2500
H7	HC	0.06	0.1255	0.2500
C5	CT	−0.12	0.2761	0.3500
H8	HC	0.06	0.1255	0.2500
H9	HC	0.06	0.1255	0.2500
C6	CT	−0.12	0.2761	0.3500
H10	HC	0.06	0.1255	0.2500
H11	HC	0.06	0.1255	0.2500
C7	CT	−0.12	0.2761	0.3500
H12	HC	0.06	0.1255	0.2500
H13	HC	0.06	0.1255	0.2500
C8	CT	−0.12	0.2761	0.3500
H14	HC	0.06	0.1255	0.2500
H15	HC	0.06	0.1255	0.2500
C9	CT	−0.12	0.2761	0.3500
H16	HC	0.06	0.1255	0.2500
H17	HC	0.06	0.1255	0.2500

continues on the next page

Atom	Atom type	Partial charge [e]	ϵ [kcal]	σ [Å]
C10	CT	−0.12	0.2761	0.3500
H18	HC	0.06	0.1255	0.2500
H19	HC	0.06	0.1255	0.2500
C11	CT	−0.12	0.2761	0.3500
H20	HC	0.06	0.1255	0.2500
H21	HC	0.06	0.1255	0.2500
C12	CT	−0.12	0.2761	0.3500
H22	HC	0.06	0.1255	0.2500
H23	HC	0.06	0.1255	0.2500
C13	CT	−0.12	0.2761	0.3500
H24	HC	0.06	0.1255	0.2500
H25	HC	0.06	0.1255	0.2500
C14	CT	−0.12	0.2761	0.3500
H26	HC	0.06	0.1255	0.2500
H27	HC	0.06	0.1255	0.2500
C15	CT	−0.12	0.2761	0.3500
H28	HC	0.06	0.1255	0.2500
H29	HC	0.06	0.1255	0.2500
C16	CT	−0.18	0.2761	0.3500
H30	HC	0.06	0.1255	0.2500
H31	HC	0.06	0.1255	0.2500
H32	HC	0.06	0.1255	0.2500

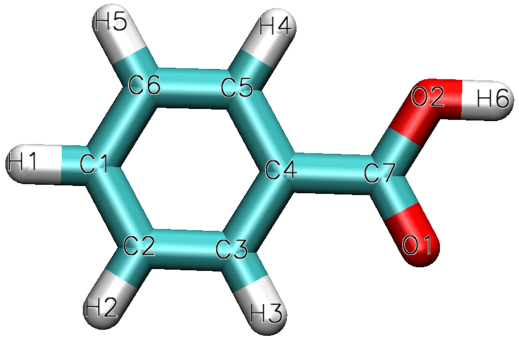

Figure 5.3: Benzoic acid molecule with atom names and numbers

Table 5.4: Atom types and corresponding parameters of the GROMOS96 54a7 force field with atomic charges and charge groups (separated by horizontal lines) used for the benzoic acid molecule

Atom	Atom type	Partial charge [e]	ϵ [kcal]	σ [Å]
C1	CA	−0.117	0.2929	0.3550
H1	HA	0.117	0.1255	0.2420
C2	CA	−0.117	0.2929	0.3550
H2	HA	0.117	0.1255	0.2420
C6	CA	−0.117	0.2929	0.3550
H5	HA	0.117	0.1255	0.2420
C3	CA	−0.138	0.2929	0.3550
H3	HA	0.138	0.1255	0.2420
C5	CA	−0.138	0.2929	0.3550
H4	HA	0.138	0.1255	0.2420
C4	CA	0.054	0.2929	0.3550
C7	C	0.579	0.4393	0.3750
O1	O_2	−0.534	0.8786	0.2960
O2	OH	−0.564	0.7113	0.3000
H6	HO	0.465	0	0

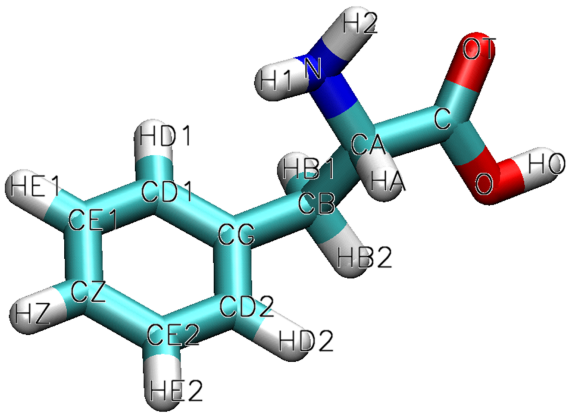

Figure 5.4: Neutral L-phenylalanine molecule with atom names and numbers

Table 5.5: Atom types and corresponding parameters of the OPLS force field, atomic charges and charge groups (separated by horizontal lines) used to parametrize the L-phenylalanine molecule

Atom	Atom type	Partial charge [e]	ϵ [kcal]	σ [Å]
CZ	CA	−0.115	0.2929	0.3550
HZ	HA	0.115	0.1255	0.2420
CE1	CA	−0.115	0.2929	0.3550
HE1	HA	0.115	0.1255	0.2420
CE2	CA	−0.115	0.2929	0.3550
HE2	HA	0.115	0.1255	0.2420
CD1	CA	−0.115	0.2929	0.3550
HD1	HA	0.115	0.1255	0.2420
CD2	CA	−0.115	0.2929	0.3550
HD2	HA	0.115	0.1255	0.2420
CG	CA	−0.115	0.2929	0.3550
CB	CT	−0.005	0.2761	0.3500
HB1	HC	0.06	0.1255	0.2500
HB2	HC	0.06	0.1255	0.2500
CA	CT_2	0.12	0.2761	0.3500
HA	HC	0.06	0.1255	0.2500
N	NT	−0.9	0.7113	0.3300
H1	H	0.36	0.0000	0.0000
H2	H	0.36	0.0000	0.0000
C	C	0.52	0.4393	0.3750
OT	O_3	−0.44	0.8786	0.2960
O	OH	−0.53	0.7113	0.3000
HO	HO	0.45	0.0000	0.0000

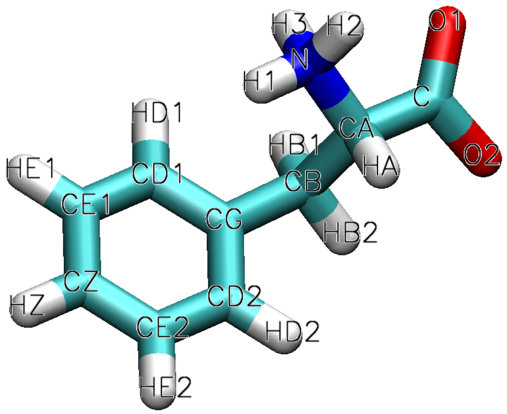

Figure 5.5: Zwitterionic L-phenylalanine with atom names and numbers

Table 5.6: Atom types and corresponding parameters of the OPLS force field, and atomic charges used to parametrize the zwitterionic L-phenylalanine molecule

Atom	Atom type	Partial charge [e]	ϵ [kcal]	σ [Å]
CZ	CA	−0.095	0.2929	0.3550
CE1	CA	−0.18	0.2929	0.3550
HE1	HA	0.151	0.1255	0.2420
CE2	CA	−0.18	0.2929	0.3550
HE2	HA	0.151	0.1255	0.2420
CD1	CA	−0.127	0.2929	0.3550
HD1	HA	0.125	0.1255	0.2420
CD2	CA	−0.127	0.2929	0.3550
HD2	HA	0.125	0.1255	0.2420
CG	CA	0.023	0.2929	0.3550
CB	CT	−0.15	0.2761	0.3500
HB1	HC	0.099	0.1255	0.2500
HB2	HC	0.099	0.1255	0.2500
CA	CT_2	0.047	0.2761	0.3500
HA	HC	0.072	0.1255	0.2500
N	N3	−0.234	0.7113	0.3250
H1	H3	0.243	0	0
H2	H3	0.243	0	0
H3	H3	0.243	0	0
C	C_3	0.74	0.4393	0.3750
HZ	HA	0.133	0.1255	0.2420
O1	O1	−0.7	0.8786	0.2960
O2	O2	−0.7	0.8786	0.2960

5.3 Appendix C - Simulation snapshots

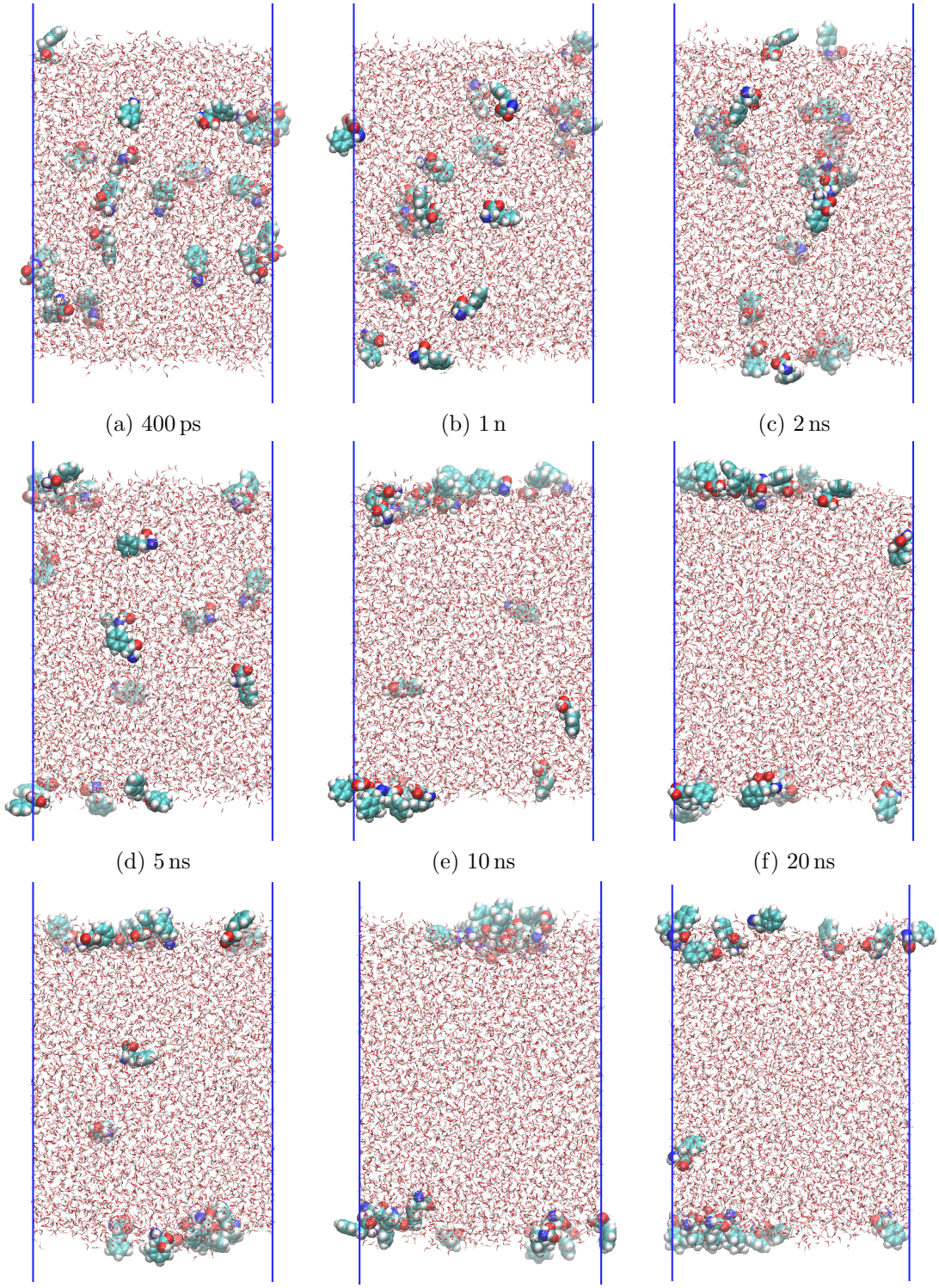

(a) 400 ps (b) 1 n (c) 2 ns

(d) 5 ns (e) 10 ns (f) 20 ns

(g) 40 ns (h) 60 ns (i) 100 ns

Figure 5.6: Time-resolved snapshots of the neutral L-phenylalanine aqueous solution NVT simulation

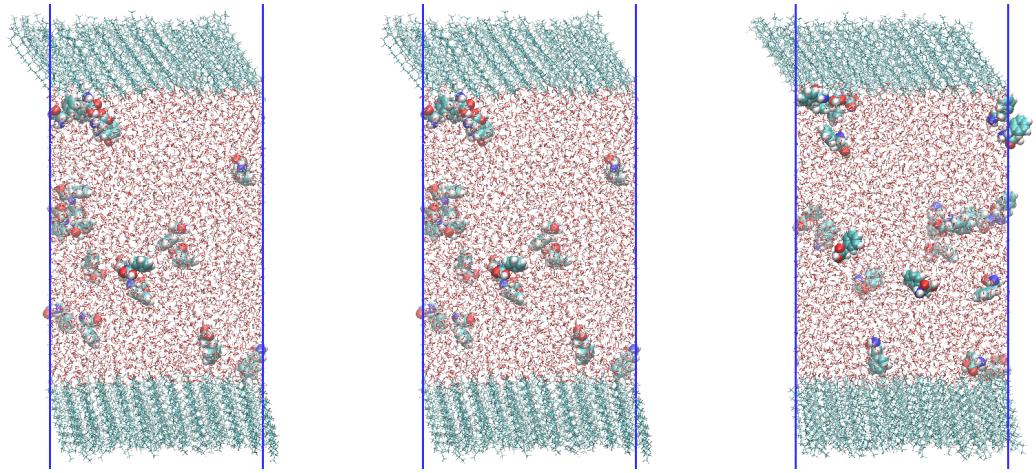

(a) 200 ps (b) 1 n (c) 2 ns

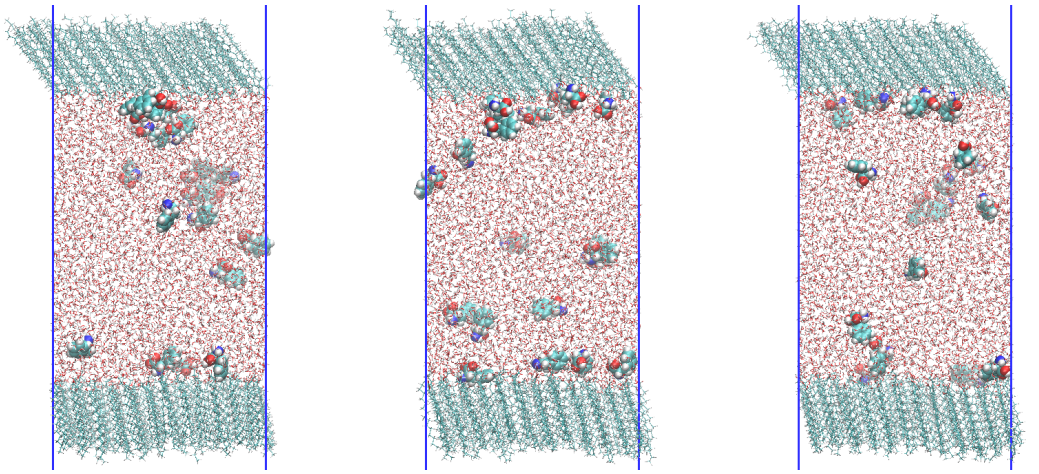

(d) 5 ns (e) 10 ns (f) 20 ns

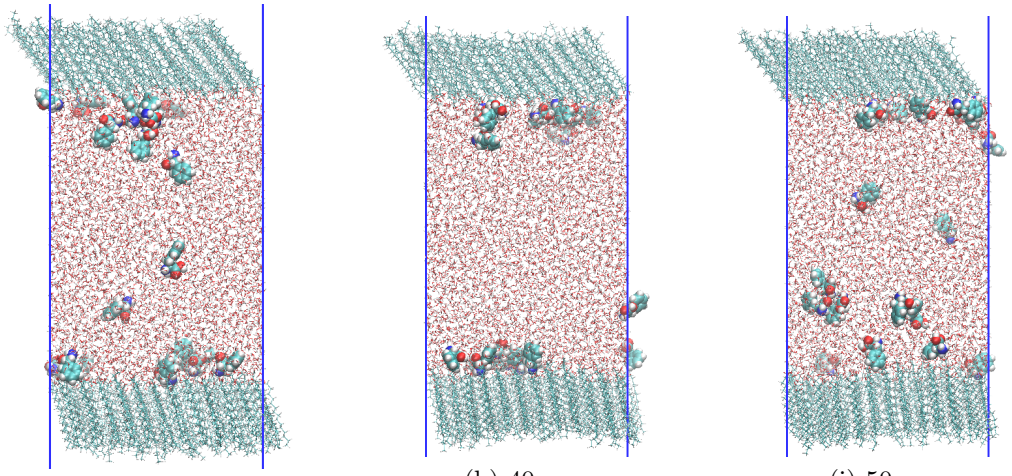

(g) 30 ns (h) 40 ns (i) 50 ns

Figure 5.7: Time-resolved snapshots of the NVT simulation of the palmitic acid monolayer in the tilted condensed phase at the neutral L-phenylalanine aqueous solution

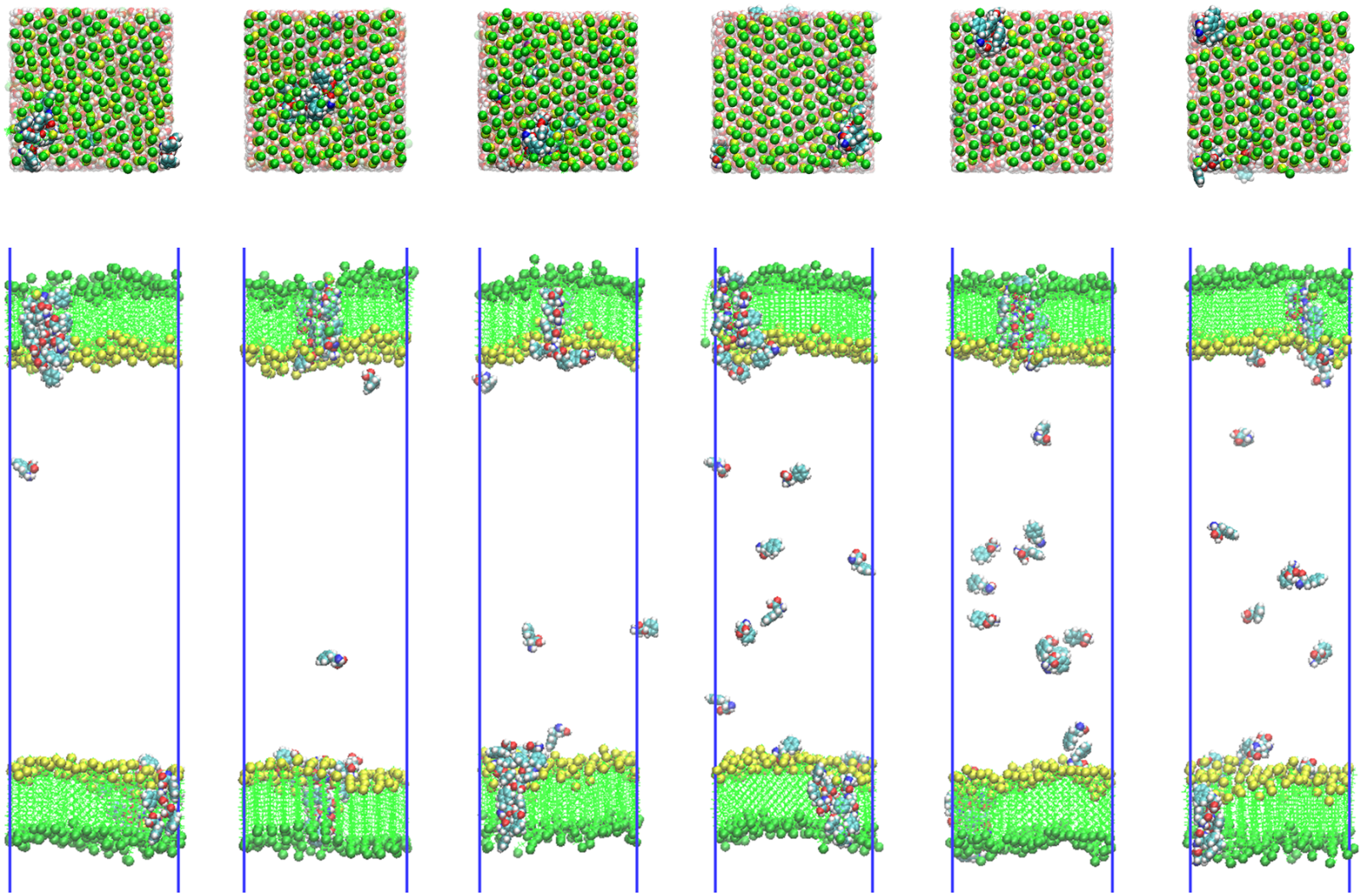

Figure 5.8: Time-resolved snapshots of the palmitic acid monolayer at the L-phenylalanine aqueous solution 200ns compression simulation at 100 bar with the 40 ns step. The aliphatic chains of the palmitic acid molecules are rendered in green, the terminal C16 atoms are shown as green beads while carboxylic headgroups as yellow beads, the water molecules between the two surfaces are not shown.

Bibliography

[1] J. L. Jimenez, M. R. Canagaratna, N. M. Donahue, A. S. H. Prevot, Q. Zhang, J. H. Kroll, P. F. DeCarlo, J. D. Allan, H. Coe, N. L. Ng, et al.: *Evolution of organic aerosols in the atmosphere*, Science **326** (2009) 1525–1529

[2] M. Kanakidou, J. H. Seinfeld, S. N. Pandis, I. Barnes, F. J. Dentener, M. C. Facchini, R. van Dingenen, B. Ervens, A. Nenes, C. J. Nielsen, et al.: *Organic aerosol and global climate modelling: A review*, Atmos. Chem. Phys. **5** (2005) 1053–1123

[3] H. Tervahattu, J. Juhanoja and K. Kupiainen: *Identification of an organic coating on marine aerosol particles by Tof-Sims*, J. Geophys. Res.: Atmos. **107** (2002) 7

[4] H. Tervahattu, J. Juhanoja, V. Vaida, A. F. Tuck, J. V. Niemi, K. Kupiainen, M. Kulmala and H. Vehkamaki: *Fatty acids on continental sulfate aerosol particles*, J. Geophys. Res.: Atmos. **110** (2005) 9

[5] I. Langmuir: *The constitution and fundamental properties of solids and liquids. II. Liquids*, J. Am. Chem. Soc. **39** (1917) 1848—1906

[6] J. A. de Gouw, A. M. Middlebrook, C. Warneke, R. Ahmadov, E. L. Atlas, R. Bahreini, D. R. Blake, C. A. Brock, J. Brioude, D. W. Fahey, et al.: *Organic aerosol formation downwind from the Deepwater Horizon oil spill*, Science **331** (2011) 1295–1299

[7] D. J. Henry, V. I. Dewan, E. L. Prime, G. G. Qiao, D. H. Solomon and I. Yarovsky: *Monolayer structure and evaporation resistance: A molecular dynamics study of octadecanol on water*, J. Phys. Chem. B **114** (2010) 3869–3878

[8] M. Hallquist, J. C. Wenger, U. Baltensperger, Y. Rudich, D. Simpson, M. Claeys, J. Dommen, N. M. Donahue, C. George, A. H. Goldstein,et al.: *The formation, properties and impact of secondary organic aerosol: current and emerging issues*, Atmos. Chem. Phys. **9** (2009) 5155–5236

[9] E. C. Griffith, T. R. C. Guizado, A. S. Pimentel, G. S. Tyndall and V. Vaida: *Oxidized aromatic-aliphatic mixed films at the air-aqueous solution interface*, J. Phys. Chem. C **117** (2013) 22341–22350

[10] E. C. Griffith, E. M. Adams, H. C. Allen and V. Vaida: *Hydrophobic collapse of a stearic acid film by adsorbed L-phenylalanine at the air-water interface*, J. Phys. Chem. B **116** (2012) 7849–7857

[11] V. M. Kaganer, M. Helmuth and P. Dutta: *Structure and phase transitions in Langmuir monolayers*, Rev. Mod. Phys. **71** (1999) 779–819

[12] S. Slančík: *Structural characterization of the interface between a fatty acid Langmuir monolayer and water using molecular simulations*, bachelor thesis supervised by RNDr. Martina Roeselová, Ph.D., Charles University in Prague (2011)

[13] R. M. Sierra-Hernández and H. C. Allen: *Incorporation and exclusion of long chain alkyl halides in fatty acid monolayers at the air-water interface*, Langmuir **26** (2010) 18806–18816

[14] A. Habartová, S. Sláčík and M. Roeselová: *manuscript in preparation*

[15] E. C. Griffith and V. Vaida: *Ionization state of L-phenylalanine at the air-water interface*, J. Am. Chem. Soc. **135** (2013) 710–716

[16] A. K. Malde, L. Zuo, M. Breeze, M. Stroet, D. Poger, P. C. Nair, C. Oostenbrink and A. E. Mark: *An Automated force field Topology Builder (ATB) and repository: version 1.0*, J. Chem. Theory Comput. **12** (2011) 4026–4037

[17] N. Schmid, A. Eichenberger, A. Choutko, S. Riniker, M. Winger, A. Mark and W. van Gunstere: *Definition and testing of the GROMOS force-field versions 54A7 and 54B7*, Eur. Biophys. J. **40** (2011) 843–856

[18] B. H. Besler, K. M. Merz Jr. and P. A. Kollman: *Atomic charges derived from semiempirical methods*, J. Comp. Chem. **11** (1990) 431–439

[19] U. C. Singh and P. A. Kollman: *An approach to computing electrostatic charges for molecules*, J. Comp. Chem. **5** (1984) 129–145

[20] C. I. Bayly, P. Cieplak, W. D. Cornell and P. A. Kollman: *A wellbehaved electrostatic potential based method using charge restraints for deriving atomic charges: the RESP model*, J. Phys. Chem. **97** (1993) 10269—10280

[21] M. J. Frisch, G. W. Trucks, H. B. Schlegel, G. E. Scuseria, M. A. Robb, J. R. Cheeseman, G. Scalmani, V. Barone, B. Mennucci, G. A. Petersson, H. Nakatsuji, M. Caricato, X. Li, H. P. Hratchian, A. F. Izmaylov, J. Bloino, G. Zheng, J. L. Sonnenberg, M. Hada, M. Ehara, K. Toyota, R. Fukuda, J. Hasegawa, M. Ishida, T. Nakajima, Y. Honda, O. Kitao, H. Nakai, T. Vreven, J. A. Montgomery, Jr., J. E. Peralta, F. Ogliaro, M. Bearpark, J. J. Heyd, E. Brothers, K. N. Kudin, V. N. Staroverov, R. Kobayashi, J. Normand, K. Raghavachari, A. Rendell, J. C. Burant, S. S. Iyengar, J. Tomasi, M. Cossi, N. Rega, J. M. Millam, M. Klene, J. E. Knox, J. B. Cross, V. Bakken, C. Adamo, J. Jaramillo, R. Gomperts, R. E. Stratmann, O. Yazyev, A. J. Austin, R. Cammi, C. Pomelli, J. W. Ochterski, R. L. Martin, K. Morokuma, V. G. Zakrzewski, G. A. Voth, P. Salvador, J. J. Dannenberg, S. Dapprich, A. D. Daniels, O. Farkas, J. B. Foresman, J. V. Ortiz, J. Cioslowski, and D. J. Fox: *Gaussian 09, Revision A.02*, Gaussian Inc., Wallingford CT (2009)

[22] Gaussian program manual online at http://www.gaussian.com/g_tech/g_ur-/g09help.htm

[23] W. L. Jorgensen: *Optimized intermolecular potential functions for liquid alcohols*, J. Phys. Chem. **90** (1986) 1276–1284

[24] H. J. C. Berendsen, J. R. Grigera and T. P. Straatsma: *The missing term in effective pair potentials*, J. Phys. Chem. **91** (1987) 6269–6271

[25] B. Hess, C. Kutzner, D. van der Spoel and E. Lindahl: *GROMACS 4: Algorithms for highly efficient, load-balanced, and scalable molecular simulation*, J. Chem. Theory Comput. **4** (2008) 435–447

[26] D. van der Spoel, E. Lindahl, B. Hess, A. R. van Buuren, E. Apol, P. J. Meulenhoff, D. P. Tieleman, A. L. T. M. Sijbers, K. A. Feenstra, R. van Drunen and H. J. C. Berendsen: *Gromacs User Manual version 4.5.6*, www.gromacs.org (2010)

[27] W. Humphrey, A. Dalke and K. Schulten: *VMD - Visual Molecular Dynamics*, J. Molec. Graphics **14** (1996) 33–38

[28] VMD program documentation online at http://www.ks.uiuc.edu/Research-/vmd/current/docs.html

[29] R. W. Hockney, S. P. Goel and J.Eastwood: *Quiet high resolution computer models of a plasma*, J. Comput. Chem. **14** (1974) 148–158

[30] L. Verlet: *Computer experiments on classical fluids. I. Thermodynamical properties of Lennard-Jones molecules*, Phys. Rev. **1459** (1967) 98–103

[31] G. Bussi, D. Donadio and M. Parrinello: *Canonical sampling through velocity rescaling*, J. Chem. Phys. **126** (2007) 014101

[32] B. Hess, H. Bekker, H. J. C. Berendsen and J. G. E. M. Fraaije: *LINCS: A linear constraint solver for molecular simulations*, J. Comput. Chem. **18** (1997) 1463—1472

[33] H. J. C. Berendsen, J. P. M. Postma, W. F. van Gunsteren, A. DiNola and J. R. Haak: *Molecular dynamics with coupling to an external bath*, J. Chem. Phys. **81** (1984) 3684

[34] U. Essman, L. Perela, M. L. Berkowitz, T. Darden, H. Lee and L. G. Pedersen: *A smooth particle mesh Ewald method*, J. Chem. Phys. **103** (1995) 8577–8592

[35] J. E. Lennard-Jones: *Cohesion*, Proc. Phys. Soc. **43** (1931) 461

[36] M. B. Plazzer, D. J. Henry, G. Yiapanis and I. Yarovsky: *Comparative study of commonly used molecular dynamics force fields for modeling organic monolayers on water*, J. Phys. Chem. B **115** (2011) 3964–3971

[37] R. L. McMullen and S. P. Kelty: *Molecular dynamic simulation of eicosanoic acid and 18-methyleicosanoic acid Langmuir monolayers*, J. Phys. Chem. B **111** (2007) 10849–10852

List of tables

List of figures

List of abbreviations

$\Pi - A$ Surface pressure – area isotherm

ATB Automated Topology Builder

BAM Brewster Angle Microscopy

GROMACS GROningen MAchine for Computer Simulations

GROMOS GROningen MOlecular Simulation

HF Hartree-Fock method

IOCB Institute of Organic Chemistry and Biochemistry of the Czech Academy of Sciences

IRRAS InfraRed Reflection-Absorption Spectroscopy

LINCS LINear Constraint Solver

MD Molecular Dynamics

MP2 Møller-Plesset second-order perturbation theory

NpT canonical ensemble with constant number of particles, pressure and temperature

NVT canonical ensemble with constant number of particles, volume and temperature

OPLS Optimized Potentials for Liquid alcoholS

PBC Periodic Boundary Conditions

PME Particle-Mesh Ewald

RESP Restrained ElectroStatic Potential

SPC/E Single Point Charge Extended

VMD Visual Molecular Dynamics